

ERROR BOUNDS FOR PHYSICS INFORMED NEURAL NETWORKS IN NONLINEAR SCHRÖDINGER EQUATIONS PLACED ON UNBOUNDED DOMAINS

MIGUEL Á. ALEJO, LUCREZIA COSSETTI, LUCA FANELLI, CLAUDIO MUÑOZ, AND NICOLÁS VALENZUELA

ABSTRACT. We consider the subcritical nonlinear Schrödinger (NLS) in dimension one posed on the unbounded real line. Several previous works have considered the deep neural network approximation of NLS solutions from the numerical and theoretical point of view in the case of bounded domains. In this paper, we introduce a new PINNs method to treat the case of unbounded domains and show rigorous bounds on the associated approximation error in terms of the energy and Strichartz norms, provided a reasonable integration scheme is available. Applications to traveling waves, breathers and solitons, as well as numerical experiments confirming the validity of the approximation are also presented as well.

1. INTRODUCTION

1.1. Setting. Among the deep learning methodologies developed in recent years, Physics-Informed Neural Networks (PINNs) have emerged as a highly relevant approach for approximating solutions to physical models using neural networks. Originally introduced in [LLF98, LBH15, RaKa18, RPP19], the PINN framework leverages the fact that deep neural networks (DNNs) possess the *universal approximation property*, i.e., the ability to approximate any continuous and even measurable function [Hor91, LLPS93, LLP00, LLF98, Yar17]. Furthermore, PINNs are able to mirror the underlying physical background of the problem, improving the modeling accuracy of DNNs.

Significant examples and advancements in the development of PINNs are provided in [RaKa18, RPP19, PLK19, MJK20, Rai18, RPK17, RyMi22, KKLPWY21]. PINNs have also been extended to solve elliptic partial differential equations (PDEs) [BDPS24, Zer22] and inverse problems [MiMo20, PeCh24]. This computational approach is now widely applied across numerous research areas, including, but not limited to, General Relativity [FMR23, LNPC24, Had23], discrete systems to uncover their underlying dynamical equations [SZC23, ZKCK22], Quantum Mechanics [WaYa21, PLC21], wave propagation [RHS22], and fiber optics [ZYX22, ZFWCQ21].

In essence, PINNs enable the use of DNNs as ansatz spaces for solving physically-driven PDEs, combining the power of neural networks with the constraints and insights provided by physical models.

In the broader context, various results demonstrate that deep neural networks are effective in approximating solutions for certain classes of PDEs. These results span both numerical and theoretical perspectives and cover a wide range of applications. Notably, the PDEs studied using these methods include linear and semilinear parabolic equations [HJE18, HaJe17, HPW20, HJKW20b, BBGJJ21, BeJe19, JSW21],

2010 *Mathematics Subject Classification.* Primary 65K10, 65M99, Secondary: 68T07.

Key words and phrases. Nonlinear Schrödinger, Physics Informed Neural Networks, Deep Neural Networks, Unbounded Domains, Solitons.

M.Á.A. was partially supported by Grant PID2022-137228OB-I00 funded by the Spanish Ministerio de Ciencia, Innovación y Universidades, MICIU/AEI/10.13039/501100011033.

L. C. was supported by the grant Ramón y Cajal RYC2021-032803-I funded by MCIN/AEI/10.13039/50110 0011033 and by the European Union NextGenerationEU/PRTR, the Deutsche Forschungsgemeinschaft (DFG, German Research Foundation) – Project-ID 258734477 – SFB 1173 and by Ikerbasque.

L. F. was supported by the projects PID2021-123034NB-I00/MCIN/AEI/10.13039/501100011033 funded by the Agencia Estatal de Investigación, IT1615-22 funded by the Basque Government, and by Ikerbasque. He is also partially supported by the Basque Government through the BERC 2022–2025 program and by the Spanish Agencia Estatal de Investigación through BCAM Severo Ochoa excellence accreditation CEX2021-001142-S/MCIN/AEI/10.13039/501100011033.

C.M. was partially funded by Chilean research grants ANID 2022 Exploration 13220060, FONDECYT 1231250, and Basal CMM FB210005.

N.V. was partially funded by Chilean research grants ANID 2022 Exploration 13220060, FONDECYT 1231250, a Latin America PhD Google Fellowship, ANID-Subdirección de Capital Humano/Doctorado Nacional/2023-21231021 and Basal CMM FB210005.

stochastic time-dependent models [GHJW18, BeJe19, BGJ20], linear and semilinear time-independent elliptic equations [LLP00, GrHe21], a variety of fluid dynamics equations [LMR20, MJK20, RJM22], and both time-dependent and time-independent non-local equations [PLK19, GRPK19, GoSc21, Val22, Val23, Cas22]. We refer to these works for further developments in this rapidly expanding research area.

Moreover, the learning methods used to achieve these results can be classified into several categories. In addition to the previously mentioned PINN technique, other prominent deep learning methods include Monte Carlo approaches [Val22, Val23, MuVa24], Multilevel Picard Iterations (MLP) [HJKW20b, BHJK20], and neural networks that approximate infinite-dimensional operators, such as DeepONets [ChCh95, LJK21, Cas23, CMV24]. Further methodologies are discussed in the recent review [BHJK23] and the monograph [JKW23].

In essence, PINNs take advantage of two key sources of data commonly available in physical systems: initial and boundary conditions, although conserved quantities may also be incorporated. In the context of classical PDEs such as Schrödinger [BKM22], Burgers, Navier-Stokes [RPK17, MJK20, RyMi22, RaKa18, LMR20, KMPT24], Kolmogorov [JSW21], and nonlinear diffusion in multiphase materials [KK24], the PINN method provides accurate numerical approximations of classical solutions.

For nonlinear dispersive PDEs, one of the key challenges in developing approximation methods arises from the fact that these equations are often posed on unbounded domains. A canonical example is the nonlinear Schrödinger equation (NLS): PINNs applied to NLS models on bounded domains were first computed in the foundational work [RPP19]. One of the earliest rigorous results in this area—using PINNs to approximate dispersive models in spatially bounded domains—was achieved in [BKM22], building on earlier work in [MiMo22].

For wave models, PINNs were used to solve the wave equation in [MMN20], and Monte Carlo methods were extended for wave models in [MuVa24]. Moreover, wave models were shown to be suitable for PINN approximation in [LBK24], including applications for approximating discontinuous solutions of nonlinear hyperbolic PDEs [RMM24]. An interesting recent paper is [JORS24bis], where an integration scheme is proposed for the integration of the cubic NLS on the 2D-torus. However, when restricting to bounded domains, many physically significant phenomena, such as the emergence of soliton-like solutions, cannot be captured.

One of the main difficulties in this field is ensuring the mathematically rigorous global validity of the PINN method for unbounded domains. To address this limitation, several improved PINN formulations and alternative neural network approaches have been proposed. For example, in problems posed on infinite domains, one computational approach involves splitting the infinite domain into finite segments using absorbing or non-reflecting boundary conditions [RRSL23, RRCWL24]. Another method employs a spectral expansion formulation [XBC23] to handle the infinite domain, where PINNs are only used to compute the unknown coefficients in the spectral expansion. Other approaches to manage unbounded domains have been explored for specific applications, such as seismic waves and thermal dynamics [RRCWL24, BaEs22].

The objective of this paper is to propose a modification to the PINN technique that enables its application to unbounded problems, specifically targeting classical soliton solutions. For simplicity, we will focus on a canonical one-dimensional dispersive model that supports the existence of solitons and breathers: the 1D-focusing NLS equation posed on the real line,

$$\begin{cases} i\partial_t u + \partial_x^2 u + |u|^{\alpha-1} u = 0, \\ u(0, \cdot) := u_0(\cdot) \in H^1(\mathbb{R}; \mathbb{C}), \end{cases} \quad (1.1)$$

where $u = u(t, x) : \mathbb{R} \times \mathbb{R} \rightarrow \mathbb{C}$, and $2 \leq \alpha < 5$, which is the natural L^2 subcritical case.* Global in time solutions in H^1 are well-known to exist [GiVe79, GiVe85, Tsu87, Bou99, Caz03, Caz89, LiPo14], due to the fact that the conserved energy

$$E(t) := \int_{\mathbb{R}} |\partial_x u(t)|^2 dx + \frac{1}{\alpha+1} \int_{\mathbb{R}} |u(t)|^{\alpha+1} dx = E(0)$$

*Some technical issues are present if $\alpha < 2$, but we believe that our results also apply to that case.

is a bound from above of the H^1 -norm. Since no boundaries exist, we will replace the boundary data by *suitable global linear data*, in the following sense. Let I be a bounded time interval containing zero. Let

$$(p, q) = \left(\frac{4(\alpha+1)}{\alpha-1}, \alpha+1 \right)$$

be Schrödinger admissible pairs (see Definition 2.1). Let

- (1) $f = f(x)$ be bounded differentiable, and $g_n = g_n(t, x)$, $n = 2, 3, 4$, bounded and continuous, both complex-valued;
- (2) Integers $N_1, N_2, N_3, N_4 \geq 1$, $M_2, M_3, M_4 \geq 1$;
- (3) For $n = 1, 2, 3, 4$, collocation points $(x_{n,j})_{j=1}^{N_n} \subseteq \mathbb{R}$, and for $n = 2, 3, 4$, times $(t_{n,\ell})_{\ell=1}^{M_n} \subseteq I$;
- (4) For $n = 1, 2, 3, 4$, vector weights $(w_{n,j})_{j=1}^{N_n} \subseteq [0, 1]$, and for $n = 2, 3, 4$, matrix weights $(w_{n,\ell,j})_{\ell,j=1}^{M_n, N_n} \subseteq [0, 1]$.

Consider the approximative norms

$$\begin{aligned} \mathcal{J}_{H^1, N_1}[f] &:= \left(\frac{1}{N_1} \sum_{j=1}^{N_1} w_{1,j} (|f(x_j)|^2 + |f'(x_j)|^2) \right)^{1/2}, \\ \mathcal{J}_{\infty, H^1, N_2, M_2}[g_2] &:= \max_{\ell=1, \dots, M_2} \left(\frac{1}{N_2} \sum_{j=1}^{N_2} w_{2,\ell,j} (|g_2(t_{2,\ell}, x_{2,j})|^2 + |\partial_x g_2(t_{2,\ell}, x_{2,j})|^2) \right)^{1/2}, \\ \mathcal{J}_{p, q, N_3, M_3}[g_3] &:= \left(\frac{1}{M_3} \sum_{\ell=1}^{M_3} \left(\frac{1}{N_3} \sum_{j=1}^{N_3} w_{3,j,\ell} |g_3(t_{3,\ell}, x_{3,j})|^q \right)^{p/q} \right)^{1/p}, \\ \mathcal{J}_{p', q', N_4, M_4}[g_4] &:= \left(\frac{1}{M_4} \sum_{\ell=1}^{M_4} \left(\frac{1}{N_4} \sum_{j=1}^{N_4} w_{4,j,\ell} |g_4(t_{4,\ell}, x_{4,j})|^{q'} \right)^{p'/q'} \right)^{1/p'}. \end{aligned} \tag{1.2}$$

The classical Riemann sums are recovered by setting the weights $w_{n,j} = 1$ and $w_{n,\ell,j} = 1$. As it is common in numerical computations, the collocation points and times will be chosen to be uniformly spaced, mimicking the standard Riemann sum. Our main result demonstrates that, under smallness assumptions on the quantities \mathcal{J}_{H^1, N_1} and $\mathcal{J}_{p', q', N_4, M_4}$ for certain functions, PINNs can satisfactorily approximate the NLS dynamics in unbounded domains.

Hypotheses on integration schemes. Following [MiMo22], our first requirement is a suitable way to approach integration.

(H1) Efficient integration. There exist efficient approximative rules for the computations of the $H_x^1(\mathbb{R})$, $L_t^\infty H_x^1(I \times \mathbb{R})$, $L_t^p W_x^{1,q}(I \times \mathbb{R})$ and $L_t^{p'} W_x^{1,q'}(I \times \mathbb{R})$ norms, in terms of the quantities defined in (1.2), in the following sense:

- For any $\delta > 0$, and all $f \in H^1(\mathbb{R})$, there exist $N_1 \in \mathbb{N}$, $R_1 > 0$, points $(x_{1,j})_{j=1}^{N_1} \subseteq [-R_1, R_1]$ and weights $(w_{1,j})_{j=1}^{N_1} \subseteq [0, 1]$ such that

$$|\|f\|_{H^1(\mathbb{R})} - \mathcal{J}_{H^1, N_1}(f)| < \delta.$$

- For any $\delta > 0$, and all $g_1 \in L_t^\infty H_x^1(I \times \mathbb{R})$, there are $N_2, M_2 \in \mathbb{N}$, $R_2 > 0$, points $(t_{2,\ell}, x_{2,j})_{j=1}^{M_2, N_2} \subseteq I \times [-R_2, R_2]$ and weights $(w_{2,\ell,j})_{\ell,j=1}^{M_2, N_2} \subseteq [0, 1]$ such that

$$|\|g_1\|_{L_t^\infty H_x^1(I \times \mathbb{R})} - \mathcal{J}_{\infty, H^1, N_2, M_2}(g_1)| < \delta.$$

- For any $\delta > 0$, and all $g_3 \in L_t^p W_x^{1,q}(I \times \mathbb{R})$, there are $N_3, M_3 \in \mathbb{N}$, $R_3 > 0$, points $(t_{3,\ell}, x_{3,j})_{j=1}^{M_3, N_3} \subseteq I \times [-R_3, R_3]$ and weights $(w_{3,\ell,j})_{\ell,j=1}^{M_3, N_3} \subseteq [0, 1]$ such that

$$|\|g_3\|_{L_t^p W_x^{1,q}(I \times \mathbb{R})} - \mathcal{J}_{p, q, N_3, M_3}(g_3)| < \delta.$$

- For any $\delta > 0$, and all $g_4 \in L_t^{p'} W_x^{1,q'}(I \times \mathbb{R})$, there are $N_4, M_4 \in \mathbb{N}$, $R_4 > 0$, points $(t_{4,\ell}, x_{4,j})_{j=1}^{M_4, N_4} \subseteq I \times [-R_4, R_4]$ and weights $(w_{4,\ell,j})_{\ell,j=1}^{M_4, N_4} \subseteq [0, 1]$ such that

$$|\|g_4\|_{L_t^{p'} W_x^{1,q'}(I \times \mathbb{R})} - \mathcal{J}_{p', q', N_4, M_4}(g_4)| < \delta.$$

Note that even though we are considering functions defined in the entire real line $x \in \mathbb{R}$, we take advantage of the fact that given any f of finite norm $\|f\|_{H^1(\mathbb{R})} < +\infty$, and tolerance δ , it is possible to find $R(\delta) > 0$ such that $\|f\|_{H^1(|x| \geq R)} < \frac{1}{2}\delta$. This allows us to restrict *the numerical integration* to a large finite interval $[-R, R]$ (notice that this does not fully address the issue of defining PINNs with boundary conditions at infinity). The same argument applies in the case of time-space norms. The previous requirements are also standard in the literature [MiMo22].

Hypotheses on PINNs. Let $u_{\text{DNN},\#} = u_{\text{DNN},\#}(t, x)$ be a smooth bounded complex-valued function constructed by means of an algorithmic procedure (either SGD or any other ML optimization procedure) and realization of a suitable PINNs, in the following sense: under the framework (1.2), one has:

(H2) Uniformly bounded large time $L_x^\infty H^1$, initial time H_x^1 and large time $L_t^p W_x^{1,q}$ control for u_0 and $u_{\text{DNN},\#}$. There are $A, \tilde{A}, B > 0$ such that the following holds. For any $N_{1,0}, N_{2,0}, N_{3,0} \geq 1$ and $M_{2,0}, M_{3,0} \geq 1$, there are $N_j \geq N_{j,0}$ and $M_j \geq M_{j,0}$ such that each approximate norm $\mathcal{J}_{H^1, N_1}[(u_0 - u_{\text{DNN},\#}(0))]$, $\mathcal{J}_{\infty, H^1, N_2, M_2}[u_{\text{DNN},\#}]$ and $\mathcal{J}_{p,q, N_3, M_3}[u_{\text{DNN},\#}]$ satisfies

$$\begin{aligned} \mathcal{J}_{H^1, N_1}[(u_0 - u_{\text{DNN},\#}(0))] &\leq \tilde{A}, \\ \mathcal{J}_{\infty, H^1, N_2, M_2}[u_{\text{DNN},\#}] &\leq A, \quad \mathcal{J}_{p,q, N_3, M_3}[u_{\text{DNN},\#}] \leq B. \end{aligned}$$

(H3) Small linear $L_t^p W_x^{1,q}$ and nonlinear $L_t^{p'} W_x^{1,q'}$ control. Given $\varepsilon > 0$, and given $N_{4,0}, N_{5,0} \geq 1$ and $M_{4,0}, M_{5,0} \geq 1$, there are $N_j \geq N_{j,0}$ and $M_j \geq M_{j,0}$ and corresponding approximative norms $\mathcal{J}_{p',q',N_4,M_4}[\mathcal{E}[u_{\text{DNN},\#}]]$ and $\mathcal{J}_{p,q,N_5,M_5}[e^{it\partial_x^2}(u_0 - u_{\text{DNN},\#}(0))]$ such that

$$\mathcal{J}_{p',q',N_4,M_4}[\mathcal{E}[u_{\text{DNN},\#}]] + \mathcal{J}_{p,q,N_5,M_5}[e^{it\partial_x^2}(u_0 - u_{\text{DNN},\#}(0))] < \varepsilon,$$

with $\mathcal{E}[u_{\#}] := i\partial_t u_{\#} + \partial_x^2 u_{\#} + |u_{\#}|^{\alpha-1} u_{\#}$. Here $e^{it\partial_x^2} f(x)$ represents the standard linear Schrödinger solution issued of initial data f at time t and position x .

Notice that $u_{\text{DNN},\#}$ may not be convergent to zero as time tends to infinity; then it is only required that, given a suitable tolerance ε , hypothesis (H3) is satisfied with computed data in the region $[-R, R]$, and with bounded local control given by (H2). Also, thanks to Strichartz estimates, the bound $\mathcal{J}_{p,q,N_5,M_5}[e^{it\partial_x^2}(u_0 - u_{\text{DNN},\#}(0))]$ may be obtained from $\mathcal{J}_{H^1, N_1}[(u_0 - u_{\text{DNN},\#}(0))] \leq \tilde{A}$ by choosing \tilde{A} sufficiently small.

Finally, recall S' as the Strichartz space introduced in Definition 2.2.

Theorem 1.1. *Let $u_0 \in H^1(\mathbb{R})$, and assume (H1). Let $A, \tilde{A}, B > 0$ be fixed numbers, and let $0 < \varepsilon < \varepsilon_1$ sufficiently small. Finally, let $u_{\text{DNN},\#}$ be a DNN satisfying (H2)-(H3). Then there exists a solution $u \in \mathcal{S}'(I \times \mathbb{R})$ to (1.1) on $I \times \mathbb{R}$ with initial datum $u_0 \in H^1(\mathbb{R})$ such that for all $R > 0$ sufficiently large and constants C ,*

$$\|u - u_{\text{DNN},\#}\|_{L_t^p W_x^{1,q}(I \times [-R, R])} \leq C(A, \tilde{A}, B)\varepsilon, \quad (1.3)$$

$$\|u - u_{\text{DNN},\#}\|_{\mathcal{S}'(I \times [-R, R])} \leq C(A, \tilde{A}, B), \quad (1.4)$$

$$\|u - u_{\text{DNN},\#}\|_{L_t^\infty H_x^1(I \times [-R, R])} \leq C(A, \tilde{A}, B). \quad (1.5)$$

The previous result indicates that PINNs satisfying the bounds (H2) and (H3) will remain close to the solution of the nonlinear Schrödinger equation (NLS) in global norms. In particular, the $L_t^p W_x^{1,q}(I \times [-R, R])$ norm remains small, where the size of the interval I is finite but arbitrary. It is important to note that smallness in the $L_t^\infty H_x^1(I \times [-R, R])$ norm cannot be achieved unless the parameter \tilde{A} is chosen to be small. Additionally, since $u_{\text{DNN},\#}$ may not converge to zero as $|x| \rightarrow \infty$, the conclusions drawn within the interval $[-R, R]$, with R arbitrary but finite, are optimal in a certain sense.

We also stress that the smallness condition (H3) on $\mathcal{J}_{p',q',N_4,M_4}[\mathcal{E}[u_{\text{DNN},\#}]]$ is standard when one studies PINNs. However, the smallness condition on $\mathcal{J}_{p,q,N_3,M_3}[e^{it\partial_x^2}(u_0 - u_{\text{DNN},\#}(0))]$ is one of the key new ingredients in this paper. This condition indicates the necessity of effectively controlling the *linear evolution* of nearby initial data when evaluated using the PINNs method. This computation is straightforward, as the linear evolution can be efficiently solved with existing numerical methods and the fact that $e^{it\partial_x^2} f$ is given by

$$\mathcal{F}_{\xi \rightarrow x}^{-1} \left(e^{-it\xi^2} \mathcal{F}_{x \rightarrow \xi}(f)(\xi) \right) = \frac{1}{(4i\pi t)^{1/2}} \int_y e^{-|x-y|^2/(4it)} f(y) dy,$$

with \mathcal{F} the standard Fourier transform. In particular, $\mathcal{J}_{p,q,N_3,M_3}[e^{it\partial_x^2}(u_0 - u_{\text{DNN},\#}(0))]$ can be easily estimated and computed. Moreover, if $\tilde{A} = O(\varepsilon)$, then the bound (H3) on $\mathcal{J}_{p',q',N_4,M_4}[\mathcal{E}[u_{\text{DNN},\#}]]$ is naturally satisfied. See Remark 3.1 for additional details.

An important advantage of Theorem 1.1 is that the hypotheses are independent of the specific PINNs considered. This means that both classical and original definitions [LLF98, LBH15, RaKa18, RPP19] are as suitable as modern contributions to the field [PLC21, PLK19], among others.

Now we will explain how Theorem 1.1 is proved. A key element in the proof is a long-time stability property specifically developed for the interaction between deep neural networks (DNNs) and the NLS case. This stability property has been extensively studied in previous years [TaVi05] (and references therein) as a tool to establish global well-posedness for critical equations. In our approach, we have drawn inspiration from this method to extend the PINNs restrictions in (H2)-(H3) to the full solution over the interval $I \times [-R, R]$, R being arbitrary. Furthermore, Theorem 1.1 remains valid for any suitable DNN optimization method, other than PINNs, that satisfies conditions (H1)-(H3).

Finally, note that (4.2) may not be satisfactory, since one would like to also achieve a small $L_t^\infty H_x^1$ norm on the error. Ensuring this is naturally challenging due to the presence of the soliton and solitary wave solutions, which evolve over time by transferring energy from compact intervals to infinity. Thus, effective control will require generalizing the standard orbital stability theory to accommodate deep learning techniques. However, we are able to present an interesting preliminary result in this direction, as seen in Corollary 6.1. Further advancements in this area will be discussed in our forthcoming work [ACM24], where we employ Monte Carlo methods to control the NLS, building on our previous results for the wave equation [MuVa24]. In particular, the finite speed of propagation suggests that the approximation method should work even better for wave than for NLS.

Organization of this work. In Section 2 we provide some standard well-posedness results for NLS in H^1 . In Section 3 we prove a short time stability result. In Section 4 we provide the main tool in this paper, a long time stability result. In Section 5 we prove the main results in this work. In Section 6 we provide numerical computations supporting our findings. Finally, in Section 7 we provide a discussion and conclusions.

Acknowledgments. C. M. would like to thank the Erwin Schrödinger Institute ESI (Vienna) where part of this work was written. N. V. thanks BCAM members for their hospitality and support during research visits in 2023 and 2024. M. Á. A. would like to thank the DIM-University of Chile, for its support and hospitality during research stays while this work was written.

2. WELL-POSEDNESS 1D-NLS WITH FOCUSING NONLINEARITY: H^1 -THEORY

In this preliminary section we examine the Cauchy problem associated to the 1D-focusing NLS (1.1). As is customary, we first show *local* well-posedness of (1.1), then *global* well-posedness follows as an easy consequence of Gagliardo-Nirenberg inequalities. In our first result we show that the problem (1.1) is locally well-posed in $H^1(\mathbb{R})$ for *any* power of the nonlinearity. To present this result, we provide the following preliminary definitions and recall some useful concepts.

Definition 2.1 (Admissible pairs). We say that a pair of exponents (p, q) is Schrödinger admissible if

$$\frac{2}{p} + \frac{n}{q} = \frac{n}{2}, \quad \begin{cases} 2 \leq q < \frac{2n}{n-2}, & \text{if } n \geq 3, \\ 2 \leq q < \infty, & \text{if } n = 2, \\ 2 \leq q \leq \infty, & \text{if } n = 1. \end{cases}$$

Lemma 2.1 (Strichartz estimates). *Let (p, q) and (\tilde{p}, \tilde{q}) Strichartz admissible pairs (cf. Definition 2.1), then the following estimates hold*

$$\|e^{it\Delta} f\|_{L_t^p L_x^q} \lesssim \|f\|_{L_x^2}, \quad (S1)$$

$$\left\| \int_{\mathbb{R}} e^{i(t-s)\Delta} g(\cdot, s) ds \right\|_{L_t^{\tilde{p}} L_x^{\tilde{q}}} \lesssim \|g\|_{L_t^{\tilde{p}'} L_x^{\tilde{q}'}}, \quad \left(\left\| \int_0^t e^{i(t-s)\Delta} g(\cdot, s) ds \right\|_{L_t^p L_x^q} \lesssim \|g\|_{L_t^{\tilde{p}'} L_x^{\tilde{q}'}} \right), \quad (S2)$$

$$\left\| \int_{\mathbb{R}} e^{it\Delta} g(\cdot, t) dt \right\|_{L_x^2} \lesssim \|g\|_{L_t^{\tilde{p}'} L_x^{\tilde{q}'}}. \quad (S3)$$

Combining (S2) and (S3) one gets

$$\left\| \int_0^t e^{i(t-s)\Delta} g(\cdot, s) ds \right\|_{L_t^p L_x^q} \lesssim \|g\|_{L_t^{\tilde{p}'} L_x^{\tilde{q}'}}. \quad (S4)$$

Definition 2.2 (Strichartz space). Let $I := [-T, T]$. We define the $\mathcal{S}'(I \times \mathbb{R})$ Strichartz norm by

$$\|u\|_{\mathcal{S}'(I \times \mathbb{R})} = \|u\|_{\mathcal{S}'} := \sup \|u\|_{L_t^p W_x^{1,q}(I \times \mathbb{R})},$$

where the supremum is taken over all 1D admissible pairs (p, q) . The associated Strichartz space $\mathcal{S}'(I \times \mathbb{R})$ is defined as the closure of the test functions under this norm.

Theorem 2.1 (Local well-posedness). *If $1 < \alpha < \infty$, then for all $u_0 \in H^1(\mathbb{R})$ there exists $T = T(\|u_0\|_{H^1(\mathbb{R})}, \alpha) > 0$ and a unique solution u of (1.1) in $\mathcal{S}'(I \times \mathbb{R})$.*

Proof. Let X_T denote the Strichartz space where to perform the fixed point argument. For all positive constants T and a we define $B_T(0, a) = \{u \in X_T : \|u\|_{X_T} \leq a\}$. For appropriate values of a and $T > 0$ we shall show that

$$\Phi(u)(t) := e^{it\partial_x^2} u_0 + i \int_0^t e^{i(t-s)\partial_x^2} |u|^{\alpha-1} u ds, \quad t \in I$$

defines a contraction map on $B_T(0, a)$. In particular, if Φ is proven to have the contracting property in $X_T = \mathcal{S}'(I \times \mathbb{R})$, then the result follows. To show that we proceed in three steps. We start considering as Strichartz space X_T the energy space $X_T = L_t^\infty H_x^1(I \times \mathbb{R})$.

Case $X_T = L_t^\infty H_x^1(I \times \mathbb{R})$: Due to the embedding $H^1(\mathbb{R}) \hookrightarrow L^\infty(\mathbb{R})$ valid in the one dimensional framework, closing the fixed point argument in X_T is almost immediate. Indeed

$$\begin{aligned} \|\Phi(u)\|_{L_t^\infty H_x^1} &\leq \|e^{it\partial_x^2} u_0\|_{L_t^\infty H_x^1} + \left\| \int_0^t e^{i(t-s)\partial_x^2} |u|^{\alpha-1} u ds \right\|_{L_t^\infty H_x^1} \\ &= \|u_0\|_{H_x^1} + \left\| \left\| \int_0^t e^{i(t-s)\partial_x^2} |u|^{\alpha-1} u ds \right\|_{H_x^1} \right\|_{L_t^\infty}, \end{aligned}$$

where here we just used that $e^{it\partial_x^2}$ is unitary in $H^1(\mathbb{R})$. Using Minkowsky, the unitarity of $e^{it\partial_x^2}$ and again the Sobolev embedding $H^1(\mathbb{R}) \hookrightarrow L^\infty(\mathbb{R})$ one has

$$\begin{aligned} \left\| \int_0^t e^{i(t-s)\partial_x^2} |u|^{\alpha-1} u ds \right\|_{H_x^1} &\leq \int_0^t \| |u|^{\alpha-1} u \|_{H_x^1} ds \\ &\leq \int_0^t \|u\|_{H_x^1} \|u\|_{L^\infty}^{\alpha-1} ds \lesssim \int_0^t \|u\|_{H_x^1}^\alpha ds. \end{aligned}$$

Using the latter in the former one gets

$$\|\Phi(u)\|_{L_t^\infty H_x^1} \lesssim \|u_0\|_{H_x^1} + T \|u\|_{L_t^\infty H_x^1}^\alpha.$$

If we assume $u \in B_T(0, a)$ in $X_T = L_t^\infty H_x^1$, namely $\|u\|_{L_t^\infty H_x^1} \leq a$ and choosing $a = 2c\|u_0\|_{H_x^1}$, where c from now on will denote the constant hidden in the symbol \lesssim , then

$$\|\Phi(u)\|_{L_t^\infty H_x^1} \leq \frac{a}{2} + Ta^\alpha.$$

If T is sufficiently small, namely $Ta^{\alpha-1} \leq 1/2$, then $\Phi: B_T(0, a) \rightarrow B_T(0, a)$. Proving that Φ is a contraction can be done similarly.

Case $X_T = L_t^\infty H_x^1 \cap L_t^{\frac{4(\alpha+1)}{\alpha-1}} W_x^{1,\alpha+1}$: [†] To close the fixed point argument in this case we only need

to estimate the $L_t^{\frac{4(\alpha+1)}{\alpha-1}} W_x^{1,\alpha+1}$ -norm of the Duhamel term. We shall see the estimate for ∇u , the estimate for u is performed similarly. Using (S2) and Hölder in space one has

$$\begin{aligned} \left\| \int_0^t e^{it\partial_x^2} |u|^{\alpha-1} \nabla u ds \right\|_{L_t^{\frac{4(\alpha+1)}{\alpha-1}} L_x^{\alpha+1}} &\lesssim \| |u|^{\alpha-1} \nabla u \|_{L_t^{\frac{4(\alpha+1)}{3\alpha+5}} L_x^{\frac{\alpha+1}{\alpha}}} \\ &\leq \left\| \|\nabla u\|_{L_x^{\alpha+1}} \|u\|_{L_x^{\alpha+1}}^{\alpha-1} \right\|_{L_t^{\frac{4(\alpha+1)}{3\alpha+5}}}. \end{aligned}$$

[†]The Strichartz space $L_t^{\frac{4(\alpha+1)}{\alpha-1}} L_x^{\alpha+1}$ is the generalisation of $L_t^8 L_x^4$ for the cubic nonlinearity $\alpha = 3$.

Notice that since $\alpha + 1 > 2$, then $H_x^1(\mathbb{R}) \hookrightarrow L_x^{\alpha+1}(\mathbb{R})$. In particular, $\|u\|_{L_x^{\alpha+1}} \leq \|u\|_{H^1}$. Using Hölder in time gives

$$\begin{aligned} \left\| \|\nabla u\|_{L_x^{\alpha+1}} \|u\|_{L_x^{\alpha+1}}^{\alpha-1} \right\|_{L_t^{\frac{4(\alpha+1)}{3\alpha+5}}} &\leq \|u\|_{L_t^\infty H_x^1}^{\alpha-1} \|\nabla u\|_{L_t^{\frac{4(\alpha+1)}{3\alpha+5}} L_x^{\alpha+1}} \\ &\leq T^\delta \|u\|_{L_t^\infty H_x^1}^{\alpha-1} \|\nabla u\|_{L_t^{\frac{4(\alpha+1)}{\alpha-1}} L_x^{\alpha+1}} \\ &\leq T^\delta \|u\|_{X_T}^\alpha, \end{aligned}$$

here δ is the Hölder conjugate exponent, namely

$$\frac{3\alpha+5}{4(\alpha+1)} = \frac{\alpha-1}{4(\alpha+1)} + \frac{1}{\delta}.$$

Notice that $\delta > 0$. This, with a similar reasoning as above, closes the fixed point argument. This intermediate step involving the Strichartz space $L_t^{\frac{4(\alpha+1)}{\alpha-1}} L_x^{\alpha+1}$ is needed to treat the 1D admissible endpoint case which is object of the next step.

Case $X_T = L_t^\infty H_x^1 \cap L_t^4 W_x^{1,\infty}$: As above we need an estimate only for the Duhamel term. In order to do that we use the Strichartz estimate (S4) with $(\tilde{p}, \tilde{q}) = (4(\alpha+1)/(3\alpha+5), (\alpha+1)/\alpha)$. More precisely, using (S4) one has

$$\begin{aligned} \left\| \int_0^t e^{i(t-s)\partial_x^2} |u|^{\alpha-1} \nabla u \right\|_{L_t^4 L_x^\infty} &\lesssim \| |u|^{\alpha-1} \nabla u \|_{L_t^{\frac{4(\alpha+1)t}{3\alpha+5}} L_x^{\frac{\alpha+1}{\alpha}}} \\ &\lesssim T^\delta \|u\|_{L_t^\infty H_x^1}^{\alpha-1} \|\nabla u\|_{L_t^{\frac{4(\alpha+1)}{\alpha-1}} L_x^{\alpha+1}}, \end{aligned} \quad (2.1)$$

where the last inequality follows from the estimate obtained in the previous step. Now to conclude we want to use interpolation: let $\theta \in (0, 1)$, then

$$\begin{aligned} \|\nabla u\|_{L_x^{\alpha+1}} &= \left(\int_{\mathbb{R}} |\nabla u|^{(\alpha+1)\theta} |\nabla u|^{(\alpha+1)(1-\theta)} \right)^{1/(\alpha+1)} \\ &\leq \|\nabla u\|_{L_x^\infty}^{\frac{\alpha-1}{\alpha+1}} \|\nabla u\|_{L_x^2}^{\frac{2}{\alpha+1}}, \end{aligned}$$

where in the last estimate we used Hölder inequality and we chose $\theta = 2/(\alpha+1)$. Using the latter to estimate $\|\nabla u\|_{L_t^{\frac{4(\alpha+1)}{\alpha-1}} L_x^{\alpha+1}}$ in (2.1) one has

$$\begin{aligned} \|\nabla u\|_{L_t^{\frac{4(\alpha+1)}{\alpha-1}} L_x^{\alpha+1}} &\leq \left\| \|\nabla u\|_{L_x^\infty}^{\frac{\alpha-1}{\alpha+1}} \|\nabla u\|_{L_x^2}^{\frac{2}{\alpha+1}} \right\|_{L_t^{\frac{4(\alpha+1)}{\alpha-1}}} \\ &\leq \|\nabla u\|_{L_t^\infty L_x^2}^{\frac{2}{\alpha+1}} \|\nabla u\|_{L_t^4 L_x^\infty}^{\frac{\alpha-1}{\alpha+1}} \leq \|u\|_{X_T}. \end{aligned}$$

Using the last estimate in (2.1) we easily close the fixed point argument.

In order to prove the theorem one observes that the pairs $(\infty, 2)$ and $(4, \infty)$ represent the endpoints of 1D admissible pairs (p, q) . Thus, the conclusion of the theorem simply follows from the interpolation inequality. \square

3. SHORT TIME STABILITY

3.1. Preliminaries. We need the following preliminary definition.

Definition 3.1 (Approximate solution). We say that $u_\#$ is an approximate solution to (1.1) if $u_\#$ satisfies the perturbed equation

$$i\partial_t u_\# + \partial_x^2 u_\# + |u_\#|^{\alpha-1} u_\# = \mathcal{E}[u_\#], \quad 1 < \alpha < 5, \quad (3.1)$$

for some error function \mathcal{E} .

In this section we aim to develop a *stability theory* for the NLS equation (1.1): we will demonstraste that an approximate solution to the NLS equation (1.1) (in the sense of Definition 3.1) does not significantly deviate from the actual solution if both the error function \mathcal{E} and the initial data error are small in a suitable sense. It is important to note that this result generalizes the property of continuous dependence on initial data, which corresponds to the special case where $\mathcal{E} = 0$, as well as the uniqueness property, which corresponds to the case $\mathcal{E} = 0$ and zero initial data error, namely $u(0) = u_\#(0)$.

3.2. Short time stability. As a first stability result we show that we can prove the existence of an exact solution u to (1.1) close enough to our approximate solution $u_\#$ of (3.1), even allowing $u_0 - u_\#(0)$ to have large energy, provided that the error $\mathcal{E}[u_\#]$ of the near solution, the near solution $u_\#$ itself and the free evolution of the perturbation $u - u_\#$ are small in suitable space-time norms. The precise statement is contained in the next lemma.

Lemma 3.1 (Short-time stability). *Let I be a fixed compact interval containing zero. Let $u_\#$ be an approximate solution to (1.1) on $I \times \mathbb{R}$ in the sense of Definition 3.1. Assume that $\|u_\#\|_{L_t^\infty H_x^1(I \times \mathbb{R})} \leq A$, for some constant $A > 0$. Let $u_0 \in H^1(\mathbb{R})$ such that*

$$\|u_0 - u_\#(0)\|_{H^1(\mathbb{R})} \leq \tilde{A},$$

for some $\tilde{A} > 0$. Assume the smallness conditions

$$\|u_\#\|_{L_t^p W_x^{1,q}(I \times \mathbb{R})} \leq \varepsilon_0, \quad (3.2)$$

$$\|e^{it\partial_x^2}(u_0 - u_\#(0))\|_{L_t^p W_x^{1,q}(I \times \mathbb{R})} \leq \varepsilon, \quad (3.3)$$

$$\|\mathcal{E}[u_\#]\|_{L_t^{p'} W_x^{1,q'}(I \times \mathbb{R})} \leq \varepsilon, \quad (3.4)$$

for some $0 < \varepsilon \leq \varepsilon_0$, with $\varepsilon_0 = \varepsilon_0(A, \tilde{A})$ a small constant and where $(p, q) = \left(\frac{4(\alpha+1)}{\alpha-1}, \alpha+1\right)$.

Then there exists a solution $u \in \mathcal{S}'(I \times \mathbb{R})$ to (1.1) on $I \times \mathbb{R}$ with initial datum $u_0 \in H^1(\mathbb{R})$ such that

$$\|u - u_\#\|_{L_t^p W_x^{1,q}(I \times \mathbb{R})} \lesssim \varepsilon, \quad (3.5)$$

$$\|(i\partial_t + \partial_x^2)(u - u_\#) + \mathcal{E}[u_\#]\|_{L_t^{p'} W_x^{1,q'}(I \times \mathbb{R})} \lesssim \varepsilon \quad (3.6)$$

$$\|u - u_\#\|_{\mathcal{S}'(I \times \mathbb{R})} \lesssim \tilde{A} + \varepsilon. \quad (3.7)$$

In particular, from (3.7) one has $\|u - u_\#\|_{L_t^\infty H_x^1(I \times \mathbb{R})} \lesssim \tilde{A} + \varepsilon$.

Remark 3.1. Notice that from the Strichartz estimate (S1), the hypothesis (3.3) is redundant if one is willing to assume also smallness of the energy of $u_0 - u_\#(0)$, namely asking for $\tilde{A} = \mathcal{O}(\varepsilon)$.

Proof of Lemma 3.1. By the well-posedness theory developed in the previous section (Theorem 2.1), we can assume that the solution u to (1.1) already exists and belongs to \mathcal{S}' . Thus to prove the result we only need to show (3.5)-(3.7) as a priori estimates. We establish these bounds for $t \geq 0$, the portion of I corresponding to $t_0 < 0$ can be treated similarly.

Let $v := u - u_\#$. Then v satisfies the following equation

$$i\partial_t v + \partial_x^2 v + f(u_\# + v) - f(u_\#) + \mathcal{E}[u_\#] = 0, \quad f(s) := |s|^{\alpha-1} s. \quad (3.8)$$

Using the integral equation associated to (3.8) one has

$$v(t) = e^{it\partial_x^2}(u_0 - u_\#(0)) + i \int_0^t e^{i(t-s)\partial_x^2} [f(u_\# + v) - f(u_\#)] ds + i \int_0^t e^{i(t-s)\partial_x^2} \mathcal{E}[u_\#] ds. \quad (3.9)$$

Let $T \in I$, we will now work on the slab $[0, T] \times \mathbb{R}$.

Using (S1) for the first term in (3.9), (S2) for the second and the third terms and then hypotheses (3.2) and (3.4) we have

$$\begin{aligned} \|v\|_{\mathcal{S}'} &\lesssim \|u_0 - u_\#(0)\|_{H_x^1} + \|f(u_\# + v) - f(u_\#)\|_{L_t^{p'} W_x^{1,q'}} + \|\mathcal{E}[u_\#]\|_{L_t^{\tilde{p}'} W_x^{1,\tilde{q}'}} \\ &\lesssim \tilde{A} + S(T) + \varepsilon, \end{aligned} \quad (3.10)$$

where we have defined

$$S(T) := \|f(u_\# + v) - f(u_\#)\|_{L_t^{p'} W_x^{1,q'}([0, T] \times \mathbb{R})}.$$

Using that $f(s) = |s|^{\alpha-1} s$ one easily has

$$|\nabla[f(u_\# + v) - f(u_\#)]| \lesssim |\nabla u_\#| |v|^{\alpha-1} + |\nabla v| |u_\#|^{\alpha-1} + |\nabla v| |v|^{\alpha-1}, \quad (3.11)$$

(for example, see [TaVi05]). Thus, in order to bound $S(t)$ we need to estimate terms of the following type $\|u|^{\alpha-1}\nabla u\|_{L_t^{p'} L_x^{q'}}$. Using the Hölder inequality one obtains

$$\begin{aligned} \|u|^{\alpha-1}\nabla u\|_{L_t^{p'} L_x^{q'}} &= \|u|^{\alpha-1}\nabla u\|_{L_t^{\frac{4(\alpha+1)}{3\alpha+5}} L_x^{\frac{\alpha+1}{\alpha}}} \leq \|\nabla u\|_{L_x^{\alpha+1}} \|u\|_{L_x^{\alpha+1}}^{\alpha-1} \|L_t^{\frac{4(\alpha+1)}{3\alpha+5}}\| \\ &\leq \|\nabla u\|_{L_t^{\frac{4(\alpha+1)}{\alpha-1}} L_x^{\alpha+1}} \|u\|_{L_t^{\frac{2(\alpha^2-1)}{\alpha+3}} L_x^{\alpha+1}}^{\alpha-1} \\ &\leq T^\delta \|\nabla u\|_{L_t^{\frac{4(\alpha+1)}{\alpha-1}} L_x^{\alpha+1}} \|u\|_{L_t^{\frac{4(\alpha+1)}{\alpha-1}} L_x^{\alpha+1}}^{\alpha-1} \\ &\leq T^\delta \|\nabla u\|_{L_t^p L_x^q} \|u\|_{L_t^p L_x^q}^{\alpha-1}, \end{aligned} \quad (3.12)$$

where δ is a Hölder conjugate exponent which is positive if $\alpha < 5$ being $\frac{2(\alpha^2-1)}{\alpha+3} < \frac{4(\alpha+1)}{\alpha-1}$. Using (3.11) and (3.12) it follows

$$\begin{aligned} S(T) &\lesssim \|\nabla u_\#|v|^{\alpha-1}\|_{L_t^{p'} L_x^{q'}} + \|\nabla v|u_\#|^{\alpha-1}\|_{L_t^{p'} L_x^{q'}} + \|\nabla v|v|^{\alpha-1}\|_{L_t^{p'} L_x^{q'}} \\ &\lesssim_T \|\nabla u_\#\|_{L_t^p L_x^q} \|v\|_{L_t^p L_x^q}^{\alpha-1} + \|\nabla v\|_{L_t^p L_x^q} \|u_\#\|_{L_t^p L_x^q}^{\alpha-1} + \|\nabla v\|_{L_t^p L_x^q} \|v\|_{L_t^p L_x^q}^{\alpha-1} \\ &\lesssim_T \|u_\#\|_{L_t^p W_x^{1,q}} \|v\|_{L_t^p W_x^{1,q}}^{\alpha-1} + \|v\|_{L_t^p W_x^{1,q}} \|u_\#\|_{L_t^p W_x^{1,q}}^{\alpha-1} + \|v\|_{L_t^p W_x^{1,q}}^\alpha. \end{aligned} \quad (3.13)$$

Using (3.2) and that

$$\begin{aligned} \|v\|_{L_t^p W_x^{1,q}} &\lesssim \|e^{it\partial_x^2}(u_0 - u_\#(0))\|_{L_t^p W_x^{1,q}} + \|f(u_\# + v) - f(u_\#)\|_{L_t^{p'} W_x^{1,q'}} + \|\mathcal{E}[u_\#]\|_{L_t^{p'} W_x^{1,q'}} \\ &\lesssim S(T) + \varepsilon, \end{aligned} \quad (3.14)$$

where in the last inequality we have used (3.3) and (3.4), from (3.13) we have

$$S(T) \lesssim_T \varepsilon_0 (S(T) + \varepsilon)^{\alpha-1} + \varepsilon_0^{\alpha-1} (S(T) + \varepsilon) + (S(T) + \varepsilon)^\alpha.$$

Taking ε_0 sufficiently small, a standard continuity argument gives

$$S(T) \leq \varepsilon, \quad \text{for all } T \in I,$$

which implies (3.6). Using this bound in (3.14) and (3.10) gives (3.5) and (3.7), respectively. Thus the proof of the lemma is concluded. \square

4. LONG TIME STABILITY

We will now focus on iterating the aforementioned result to address the more general scenario of near-solutions with *finite* yet *arbitrarily large* space-time norms. Specifically, our objective is to prove the following alternative lemma.

Lemma 4.1 (Long-time stability). *Let I be a fixed compact interval containing zero. Let $u_\#$ be an approximate solution to (1.1) on $I \times \mathbb{R}$ in the sense of Definition 3.1. Assume that*

$$\|u_\#\|_{L_t^\infty H_x^1(I \times \mathbb{R})} \leq A, \quad (4.1)$$

for some constant $A > 0$. Let $u_0 \in H^1(\mathbb{R})$ such that

$$\|u_0 - u_\#(0)\|_{H^1(\mathbb{R})} \leq \tilde{A}, \quad (4.2)$$

for some $\tilde{A} > 0$. Assume

$$\|u_\#\|_{L_t^p W_x^{1,q}(I \times \mathbb{R})} \leq B, \quad (4.3)$$

$$\|e^{it\partial_x^2}(u_0 - u_\#(0))\|_{L_t^p W_x^{1,q}(I \times \mathbb{R})} \leq \varepsilon, \quad (4.4)$$

$$\|\mathcal{E}[u_\#]\|_{L_t^{p'} W_x^{1,q'}(I \times \mathbb{R})} \leq \varepsilon, \quad (4.5)$$

for some constant $B > 0$, $0 < \varepsilon \leq \varepsilon_1$, with $\varepsilon_1 = \varepsilon_1(A, \tilde{A}, B) > 0$ a small constant, where $(p, q) = \left(\frac{4(\alpha+1)}{\alpha-1}, \alpha+1\right)$.

Then there exists a unique solution $u \in \mathcal{S}'(I \times \mathbb{R})$ to (1.1) on $I \times \mathbb{R}$ with initial data $u_0 \in H^1(\mathbb{R})$ such that

$$\|u - u_\#\|_{L_t^p W_x^{1,q}(I \times \mathbb{R})} \leq C(A, \tilde{A}, B) \varepsilon, \quad (4.6)$$

$$\|u - u_\#\|_{\mathcal{S}'(I \times \mathbb{R})} \leq C(A, \tilde{A}, B). \quad (4.7)$$

In particular, from (4.7) one has $\|u - u_{\#}\|_{L_t^{\infty} H_x^1(I \times \mathbb{R})} \leq C(A, \tilde{A}, B)$.

Lemma 4.1 can be obtained as an easy consequence of Lemma 3.1 just using an iteration argument based on partitioning the time interval.

Proof of Lemma 4.1. Without loss of generality we may assume that $t_0 := 0$ is the lower bound of the interval I . Let $\varepsilon_0 = \varepsilon_0(A, 2\tilde{A})$ be as in Lemma 3.1. Since from (4.3) the $L_t^p W_x^{1,q}(I \times \mathbb{R})$ norm of $u_{\#}$ is finite, we can subdivide the interval I into $N \leq C(A, B, \varepsilon_0)$ sub-intervals $I_j = [t_j, t_{j+1}]$ such that on each I_j we have

$$\|u_{\#}\|_{L_t^p W_x^{1,q}(I_j \times \mathbb{R})} \leq \varepsilon_0. \quad (4.8)$$

Choosing ε_1 sufficiently small depending on ε_0, N, A and \tilde{A} , we can apply Lemma 3.1 to obtain that for each $j \in \{0, \dots, N-1\}$ then we have

$$\begin{aligned} \|u - u_{\#}\|_{L_t^p W_x^{1,q}(I_j \times \mathbb{R})} &\lesssim_j \varepsilon, \\ \|u - u_{\#}\|_{\mathcal{S}'(I_j \times \mathbb{R})} &\lesssim_j \tilde{A} + \varepsilon, \end{aligned} \quad (4.9)$$

provided we can show that the smallness assumptions (4.4) and (4.5) hold with $t_0 = 0$ replaced by the lower bound t_j of the sub-interval I_j . First of all one observes that by an inductive argument

$$S(t_l) := \|(i\partial_t + \partial_x^2)(u - u_{\#}) + \mathcal{E}[u_{\#}]\|_{L_t^p W_x^{1,q}(I_l \times \mathbb{R})} \leq C(l)\varepsilon,$$

for any $l \in \{0, N-1\}$. From Lemma 3.1 applied to $I_0 = [0, t_1]$, one has $S(t_0) \leq \varepsilon$ (cf. (3.6)). Arguing as in the proof of Lemma 3.1, for $l \in \{1, N-1\}$ we get

$$S(t_l) \leq \sum_{k=1}^{\alpha} \|v\|_{L_t^p W_x^{1,q}([0, t_{l+1}] \times \mathbb{R})}^k \|u_{\#}\|_{L_t^p W_x^{1,q}(I_l \times \mathbb{R})}^{\alpha-k}. \quad (4.10)$$

From the integral equation (3.9) one has

$$\begin{aligned} &\|v\|_{L_t^p W_x^{1,q}([0, t_{l+1}] \times \mathbb{R})} \\ &\leq \|e^{it\partial_x^2}(u_0 - u_{\#}(0))\|_{L_t^p W_x^{1,q}([0, t_{l+1}] \times \mathbb{R})} + \|(i\partial_t + \partial_x^2)(u - u_{\#}) + \mathcal{E}[u_{\#}]\|_{L_t^{p'} W_x^{1,q'}([0, t_{l+1}] \times \mathbb{R})} \\ &\quad + \|\mathcal{E}[u_{\#}]\|_{L_t^{p'} W_x^{1,q'}(I \times \mathbb{R})} \\ &\leq \|e^{it\partial_x^2}(u_0 - u_{\#}(0))\|_{L_t^p W_x^{1,q}([0, t_{l+1}] \times \mathbb{R})} + \sum_{m=0}^{l-1} S(t_m) + S(t_l) + \|\mathcal{E}[u_{\#}]\|_{L_t^{p'} W_x^{1,q'}(I \times \mathbb{R})} \\ &\leq C(l)(S(t_l) + \varepsilon), \end{aligned}$$

where the last bound follows from (4.4), (4.5) and the inductive hypothesis $S(t_m) \leq C(m)\varepsilon$ for any $m \in \{0, l-1\}$. Plugging this bound in (4.10), using also (4.8), then a continuity argument as above gives

$$S(t_l) \leq C(l)\varepsilon. \quad (4.11)$$

Now, using (3.9), by the unitarity in H_x^1 of the operator $e^{it\partial_x^2}$ and from Strichartz estimate (S4) one has

$$\begin{aligned} \|u(t_j) - u_{\#}(t_j)\|_{H_x^1(\mathbb{R})} &\leq \|u(t) - u_{\#}(t)\|_{L_t^{\infty} H_x^1([0, t_j] \times \mathbb{R})} \\ &\leq \|u_0 - u_{\#}(0)\|_{H_x^1(\mathbb{R})} + \sum_{l=0}^{j-1} S(t_l) + \|\mathcal{E}[u_{\#}]\|_{L_t^{p'} W_x^{1,q'}(I \times \mathbb{R})} \\ &\lesssim \tilde{A} + \varepsilon + \sum_{l=0}^{j-1} C(l)\varepsilon, \end{aligned}$$

where the last bound follows from (4.2), (4.5) and (4.11).

Similarly, one has

$$\begin{aligned}
& \|e^{i(t-t_j)\partial_x^2}(u(t_j) - u_{\#}(t_j))\|_{L_t^p W_x^{1,q}(I_j \times \mathbb{R})} \\
& \leq \|e^{it\partial_x^2}(u_0 - u_{\#}(0))\|_{L_t^p W_x^{1,q}([0, t_{j+1}] \times \mathbb{R})} + \left\| \int_0^{t_j} e^{i(t-s)\partial_x^2}(i\partial_t + \partial_x^2)(u - u_{\#}) ds \right\|_{L_t^p W_x^{1,q}([0, t_{j+1}] \times \mathbb{R})} \\
& \leq \|e^{it\partial_x^2}(u_0 - u_{\#}(0))\|_{L_t^p W_x^{1,q}([0, t_{j+1}] \times \mathbb{R})} + \sum_{l=0}^j S(t_l) + \|\mathcal{E}[u_{\#}]\|_{L_t^{p'} W_x^{1,q'}(I \times \mathbb{R})} \\
& \leq \varepsilon + \sum_{l=0}^j C(l)\varepsilon.
\end{aligned}$$

Choosing ε_1 sufficiently small, one has that (4.9) holds true for any $j \in \{0, \dots, N-1\}$. Thus, bounds (4.6) and (4.7) follow summing over all the intervals I_j , $j \in \{0, \dots, N-1\}$. \square

5. PROOF OF THE MAIN RESULT

Consider an interval of time I containing zero. Let $u_0 \in H^1(\mathbb{R})$. Assume (H1). Let $A, \tilde{A}, B > 0$ be fixed values. Let $0 < \varepsilon < \varepsilon_1(A, \tilde{A}, B)$. Recall

$$(p, q) = \left(\frac{4(\alpha+1)}{\alpha-1}, \alpha+1 \right).$$

Let $u(t)$ be the corresponding solution to NLS with initial data u_0 . Let $u_{\text{DNN},\#}$ be the realization of a DNN $\Phi_{\#}$ as in Theorem 1.1, such that (H2) and (H3) are satisfied in the following sense:

(Step 1) For N_1, N_2, N_3 and M_2, M_3 sufficiently large, collocation points, times and weights, one has

$$\mathcal{J}_{\infty, H^1, N_2, M_2}[u_{\text{DNN},\#}] \leq \frac{1}{2}A, \quad \mathcal{J}_{H^1, N_1}[(u_0 - u_{\text{DNN},\#}(0))] \leq \frac{1}{2}\tilde{A}, \quad \mathcal{J}_{p, q, N_3, M_3}[u_{\text{DNN},\#}] \leq \frac{1}{2}B.$$

Later we will choose specific values for the parameters of the approximative norms. Similarly, we will require as well that

(Step 2) For all N_4, M_4 and N_5, M_5 positive integers large enough, collocation points, times and weights,

$$\mathcal{J}_{p', q', N_4, M_4}[\mathcal{E}[u_{\text{DNN},\#}]] + \mathcal{J}_{p, q, N_5, M_5}[e^{it\partial_x^2}(u_0 - u_{\text{DNN},\#}(0))] < \frac{1}{2}\varepsilon,$$

$$\text{with } \mathcal{E}[u_{\#}] := i\partial_t u_{\#} + \partial_x^2 u_{\#} + |u_{\#}|^{\alpha-1} u_{\#}.$$

Let

$$R := \max_{n=1,2,3,4} \max_{j=1, \dots, N_1} \{|x_{n,j}|\}$$

be the maximum modulus of evaluation/collocation points among all the previous approximate integrals. Let $[-R, R] \subseteq \mathbb{R}$. Let $\eta_R \in C_0^\infty(\mathbb{R})$, $0 \leq \eta \leq 1$, be a cut-off function such that $\eta = 1$ in $[-R, R]$ and $\eta(x) = 0$ if $|x| \geq 2R$. Define $u_{\#} := u_{\text{DNN},\#} \eta_R$ now in Sobolev and Lebesgue spaces. Note that for all $t \in I$, and all $x \in [-R, R]$, one has $u_{\#} = u_{\text{DNN},\#}$. Consequently,

$$\begin{aligned}
\mathcal{J}_{\infty, H^1, N_2, M_2}[u_{\text{DNN},\#}] &= \mathcal{J}_{\infty, H^1, N_2, M_2}[u_{\#}], \\
\mathcal{J}_{H^1, N_1}[(u_0 - u_{\text{DNN},\#}(0))] &= \mathcal{J}_{H^1, N_1}[(u_0 - u_{\#}(0))], \quad \mathcal{J}_{p, q, N_3, M_3}[u_{\text{DNN},\#}] = \mathcal{J}_{p, q, N, M}[u_{\#}],
\end{aligned}$$

and

$$\mathcal{J}_{p', q', N_4, M_4}[\mathcal{E}[u_{\text{DNN},\#}]] = \mathcal{J}_{p', q', N_4, M_4}[\mathcal{E}[u_{\#}]],$$

$$\mathcal{J}_{p, q, N_5, M_5}[e^{it\partial_x^2}(u_0 - u_{\text{DNN},\#}(0))] = \mathcal{J}_{p, q, N_5, M_5}[e^{it\partial_x^2}(u_0 - u_{\#}(0))].$$

Now (modulo choosing N_j, M_j once again larger, and R larger if necessary, which does not affect the last identities) we can use hypothesis (H1) and choose particular integration parameters for $f = u_0 - u_{\#}(0)$ and $\delta = \frac{1}{2}\varepsilon$ to get

$$\|u_0 - u_{\#}(0)\|_{H^1(\mathbb{R})} \leq \mathcal{J}_{H^1, N_1}[(u_0 - u_{\#}(0))] + \frac{1}{2}\varepsilon.$$

Similarly, for $g_2 = g_3 = u_{\#}$ and $\delta = \frac{1}{2}\varepsilon$, we choose integration parameters such that

$$\|u_{\#}\|_{L_t^\infty H^1(I \times \mathbb{R})} \leq \mathcal{J}_{\infty, H^1, N_2, M_2}[u_{\#}] + \frac{1}{2}\varepsilon,$$

$$\|u_{\#}\|_{L_t^p W_x^{1,q}(I \times \mathbb{R})} \leq \mathcal{J}_{p, q, N_3, M_3}[u_{\#}] + \frac{1}{2}\varepsilon.$$

Therefore,

$$\begin{aligned}\|u_0 - u_{\#}(0)\|_{H^1(\mathbb{R})} &\leq \mathcal{J}_{H^1, N_1}[(u_0 - u_{\text{DNN}, \#}(0))] + \frac{1}{2}\varepsilon \leq \frac{1}{2}(\tilde{A} + \varepsilon) \leq \tilde{A}, \\ \|u_{\#}\|_{L_t^{\infty} H^1(I \times \mathbb{R})} &\leq \mathcal{J}_{\infty, H^1, N_2, M_2}[u_{\text{DNN}, \#}] + \frac{1}{2}\varepsilon \leq \frac{1}{2}(A + \varepsilon) \leq A, \\ \|u_{\#}\|_{L_t^p W_x^{1,q}(I \times \mathbb{R})} &\leq \mathcal{J}_{p, q, N_3, M_3}[u_{\text{DNN}, \#}] + \frac{1}{2}\varepsilon \leq \frac{1}{2}(B + \varepsilon) \leq B.\end{aligned}$$

Additionally, using again the Hypothesis (H1),

$$\begin{aligned}\|\mathcal{E}[u_{\#}]\|_{L_t^{p'} W_x^{1,q'}(I \times \mathbb{R})} &\leq \mathcal{J}_{p', q', N_4, M_4}[\mathcal{E}[u_{\text{DNN}, \#}]] + \frac{1}{2}\varepsilon \leq \frac{1}{2}\varepsilon + \frac{1}{2}\varepsilon = \varepsilon, \\ \|e^{it\partial_x^2}(u_0 - u_{\#}(0))\|_{L_t^p W_x^{1,q}(I \times \mathbb{R})} &\leq \mathcal{J}_{p, q, N_5, M_5}[e^{it\partial_x^2}(u_0 - u_{\text{DNN}, \#}(0))] + \frac{1}{2}\varepsilon \leq \frac{1}{2}\varepsilon + \frac{1}{2}\varepsilon = \varepsilon.\end{aligned}$$

The hypotheses (4.1)-(4.5) in Lemma 4.1 are satisfied and one has that there exists a solution $u \in \mathcal{S}'(I \times \mathbb{R})$ to (1.1) on $I \times \mathbb{R}$ with initial data $u_0 \in H^1(\mathbb{R})$ such that

$$\begin{aligned}\|u - u_{\#}\|_{L_t^p W_x^{1,q}(I \times \mathbb{R})} &\leq C(A, \tilde{A}, B)\varepsilon, \\ \|u - u_{\#}\|_{\mathcal{S}'(I \times \mathbb{R})} &\leq C(A, \tilde{A}, B), \\ \|u - u_{\#}\|_{L_t^{\infty} H_x^1(I \times \mathbb{R})} &\leq C(A, \tilde{A}, B).\end{aligned}$$

The final conclusion (1.3)-(1.4)-(1.5) are obtained after considering the subinterval $[-R, R]$ and recalling that $u_{\#} = u_{\text{DNN}, \#}$ in this interval.

6. NUMERICAL RESULTS

6.1. Application to Solitary waves. Theorem 1.1 establishes a rigorous framework for the approximation of NLS solitons. Solitary waves are a fundamental aspect of the focusing NLS equation [Caz03]. When $\alpha = 3$, the NLS becomes integrable, and exhibits solitons, multisolitons, and breather solutions. For a detailed exploration of these phenomena, see [Caz03, Caz89, AFM21, AFM20, AC24, SY74]. Additionally, for more information on breather solutions in other models, references such as [Wad73, AM13, BMW94, AMP17] provide further insight.

Corollary 6.1. *Let $\alpha \in [2, 5]$ and $\varepsilon > 0$. Let $u(t) \in H^1(\mathbb{R})$ be any NLS solitary wave solution; or soliton, multi-soliton or breather if $\alpha = 3$. Then there is $\tilde{A} = \tilde{A}(\varepsilon, I) = o_{\varepsilon}(1)$, such that the following holds. Assume that $u_{\text{DNN}, \#}$ is a DNN-generated realization of a PINNs Φ such that (H1)-(H3) are satisfied with \tilde{A} as above. Then for all $R > 0$ sufficiently large,*

$$\|u - u_{\text{DNN}, \#}\|_{L_t^{\infty} H_x^1(I \times [-R, R])} \lesssim_{A, B} \varepsilon.$$

The proof of this fact immediately follows from Remark 3.1 and the continuity of the flow. It is an open question to introduce and mix standard stability techniques in the description of PDEs via PINNs. Although Corollary 6.1 may be considered as a consequence of the continuity of the flow, we will argue below that numerical tests corroborate Theorem 1.1 and the “long time stability” nature of the approximate PINNs solutions.

6.2. Numerical tests. Preliminaries. We conducted numerical tests to validate Theorem 1.1 and Corollary 6.1, specifically focusing on well-known NLS solitary waves. All the codes are available in <https://github.com/nvalenzuelaf/DNN-Pinns-NLS> and the simulations were carried out using Python on a 64-bit MacBook Pro M2 (2022) with 8GB of RAM.

For these tests, we selected the integrable case of $\alpha = 3$, where many explicit soliton solutions are available. In this scenario, the chosen exponents are $(p, q) = (8, 4)$, with the Hölder conjugates being $p' = \frac{8}{7}$ and $q' = \frac{4}{3}$. Our goal was to numerically approximate the solution $u_{\text{DNN}, \#}$ using an algorithm implemented in Python. The full details of the algorithm are as follows:

- (i) We start with a DNN $u_{\text{DNN}, \#} := u_{\text{DNN}, \#, \theta}$ having 4 hidden layers, 20 neurons per layer and the classical sine activation function acting component-wise. The weights and biases will be initialized in a standard way, using the Glorot uniform initializer. They will be summarized in θ as the optimization variables.
- (ii) To optimize the DNN parameters, we will use the LBFGS method (see, e.g. [Fle13, KoWh19]), which in our case performed better than the standard Adam method, with 3000 iterations.

(iii) For N_4, M_4, N_5, M_5 as in (H3) we choose the points $(x_{4,j})_{j=1}^N, (x_{5,j})_{j=1}^{N_5} \subset [-R, R]$, and $(t_{4,\ell})_{\ell=1}^{M_4}, (t_{5,\ell})_{\ell=1}^{M_5} \subset [-T, T]$ to obtain two grids of $M_4 \times N_4$ and $M_5 \times N_5$ points $(t_{4,\ell}, x_{4,j})_{\ell,j=1}^{M_4, N_4}$ and $(t_{5,\ell}, x_{5,j})_{\ell,j=1}^{M_5, N_5}$, respectively.

Unless we say the opposite, we will take in the numerical simulations $N_4 = N_5 = M_4 = M_5 = 32$, and $(x_{4,j})_{j=1}^{N_4} = (x_{5,j})_{j=1}^{N_5}$, $(t_{4,\ell})_{\ell=1}^{M_4} = (t_{5,\ell})_{\ell=1}^{M_5}$ will be taken as uniformly partitions over $[-R, R]$ and $[-T, T]$, respectively.

(iv) We will consider the loss function as the functions defined in (H3): First, for simplicity define

$$v(t, \cdot) \equiv e^{it\partial_x^2} (u_0 - u_{\text{DNN}, \#}(0)).$$

As said before, this linear evolution can be computed using an approximation on the corresponding Fourier transform. Denote as $\hat{v}(t_\ell, x_j)$ the approximation of v at the point (t_ℓ, x_j) . Then the loss function takes the form:

$$\begin{aligned} \text{Loss}(\theta) &:= \mathcal{J}_{p', q', N_4, M_4} [\mathcal{E}[u_{\text{DNN}, \#}]] + \mathcal{J}_{p, q, N_5, M_5} [\hat{v}] \\ &= \left(\frac{1}{M_4} \sum_{\ell=1}^{M_4} \left(\frac{1}{N_4} \sum_{j=1}^{N_4} |\mathcal{E}[u_{\text{DNN}, \#}](\hat{t}_\ell, \hat{x}_j)|^{q'} \right)^{\frac{p'}{q'}} \right)^{\frac{1}{p'}} + \left(\frac{1}{M_5} \sum_{\ell=1}^{M_5} \left(\frac{1}{N_5} \sum_{j=1}^{N_5} |\hat{v}(t_\ell, x_j)|^q \right)^{\frac{p}{q}} \right)^{\frac{1}{p}}, \end{aligned} \quad (6.1)$$

where we recall $\mathcal{E}[u_{\text{DNN}, \#}] := i\partial_t u_{\text{DNN}, \#} + \partial_x^2 u_{\text{DNN}, \#} + |u_{\text{DNN}, \#}|^{\alpha-1} u_{\text{DNN}, \#}$.

(v) In each example we aim to obtain numeric values for the bounds involved in (H2). For this, along this section we consider in each iteration step the quantities

$$\tilde{A} := \mathcal{J}_{H^1, N_1} [(u_0 - u_{\text{DNN}, \#}(0))],$$

$$A := \mathcal{J}_{\infty, H^1, N_2, M_2} [u_{\text{DNN}, \#}], \quad B := \mathcal{J}_{p, q, N_3, M_3} [u_{\text{DNN}, \#}],$$

where $u_{\text{DNN}, \#}$ is the respective DNN of each iteration in the LBFGS algorithm and $N_1 = N_2 = N_3 = N_5$ and $M_2 = M_3 = M_5$.

(vi) Consider $N_{\text{test}} = M_{\text{test}} = 100$. We will use as test data a grid of $N_{\text{test}} \times M_{\text{test}}$ points $(t_\ell, x_j)_{\ell,j=1}^{M_{\text{test}}, N_{\text{test}}}$ generated in the same way as the training points. If $u = u(t, x)$ is the exact solution of the NLS equation, we will compute the following errors

$$\text{error}_{\mathcal{S}'} := \max_{(p, q)} \mathcal{J}_{p, q, N_{\text{test}}, M_{\text{test}}} [u_{\text{DNN}, \#} - u], \quad (6.2)$$

$$\text{error}_{L_t^p W_x^{1,q}} := \mathcal{J}_{p, q, N_{\text{test}}, M_{\text{test}}} [u_{\text{DNN}, \#} - u], \quad (6.3)$$

$$\text{error}_{L_t^\infty H^1} := \mathcal{J}_{\infty, H^1, N_{\text{test}}, M_{\text{test}}} [u_{\text{DNN}, \#} - u], \quad (6.4)$$

where in (6.2) we take the maximum over a suitable grid of values of q that makes the pair (p, q) Schrödinger admissible and $(p, q) = (8, 4)$ in (6.3).

Remark 6.1 (On the approximation of $v(t, \cdot)$). Recall that $v(t, \cdot)$ is given by

$$\mathcal{F}_{\xi \rightarrow x}^{-1} \left(e^{-it\xi^2} \mathcal{F}_{x \rightarrow \xi} (u_0 - u_{\text{DNN}, \#}(0))(\xi) \right).$$

We will approximate $v(t_\ell, x_j)$ by using the `fft` package in Pytorch, that uses the fast Fourier transform (FFT) to obtain a numerical approximation of the (continuous) Fourier transform $\mathcal{F}_{x \rightarrow \xi}$ and its inverse $\mathcal{F}_{\xi \rightarrow x}^{-1}$. Thus the value of $\hat{v}(t_\ell, x_j)$ can be obtained naturally by the FFT approximation of the Fourier transform and its inverse in the definition of $v(t_\ell, x_j)$.

6.3. List of solitary waves. Following [AFM21], let $c, \nu > 0$ be fixed scaling parameters. The considered solutions will be: the solitary wave

$$Q(t, x) = e^{i\frac{\nu}{2}x - i\left(\frac{\nu^2}{4} - c\right)t} \sqrt{2c} \operatorname{sech}(\sqrt{c}(x - \nu t)). \quad (6.5)$$

(notice that if $\nu = 0$, then the solitary-wave solution remains to a standing wave solution), the Peregrine breather [Per83]

$$B_{\text{P}}(t, x) := e^{it} \left(1 - \frac{4(1 + 2it)}{1 + 4t^2 + 2x^2} \right), \quad (6.6)$$

and the Kuznetsov-Ma (KM) breather [Kuz77, Ma79]

$$B_{\text{KM}}(t, x) := e^{it} \left(1 - \sqrt{2} \tilde{\beta} \frac{\tilde{\beta}^2 \cos(\tilde{\alpha}t) + i\tilde{\alpha} \sin(\tilde{\alpha}t)}{\tilde{\alpha} \cosh(\tilde{\beta}x) - \sqrt{2}\tilde{\beta} \cos(\tilde{\alpha}t)} \right), \quad (6.7)$$

with

$$\tilde{\alpha} := (8a(2a-1))^{\frac{1}{2}}, \quad \tilde{\beta} := (2(2a-1))^{\frac{1}{2}}, \quad a > \frac{1}{2},$$

Notice that the KM breather does not converge to zero at infinity, but after the subtraction of the background, it becomes a localized solution. The stability of the KM breather (and other breathers) has been studied in [Mu17, AFM19, AFM21]. Additionally, if $\alpha \in (1, 5)$, $\alpha \neq 3$, and $\omega > 0$, we shall consider the standing wave solution

$$u_{\omega}(t, x) = e^{i\omega t} \left(\left(\frac{\alpha+1}{2} \right) \omega \operatorname{sech}^2 \left(\frac{\alpha-1}{2} \sqrt{\omega} x \right) \right)^{\frac{1}{\alpha-1}}. \quad (6.8)$$

We have chosen $N = 100$ and $M = 100$ in every error computation, representing a grid of 10^4 space-time evaluation points. The training data will be the exact soliton or solitary wave solution evaluated at 32×32 points for each member in (6.1).

6.4. Solitons. We present now our first results for the case of the soliton Q in (6.5). We choose parameters $c = \nu = 1$ but we ensure that our results are very similar for other similar values of c and ν . The space region is $[-8, 8]$ and the time region $[-2, 2]$. Our results are summarized in Fig. 1, where the continuous line represents the exact solution and the dashed line is the solution computed using the proposed PINNs minimization procedure. In particular, Fig. 1a and 1b present respectively the real and imaginary parts of the computed soliton solution for three different times.

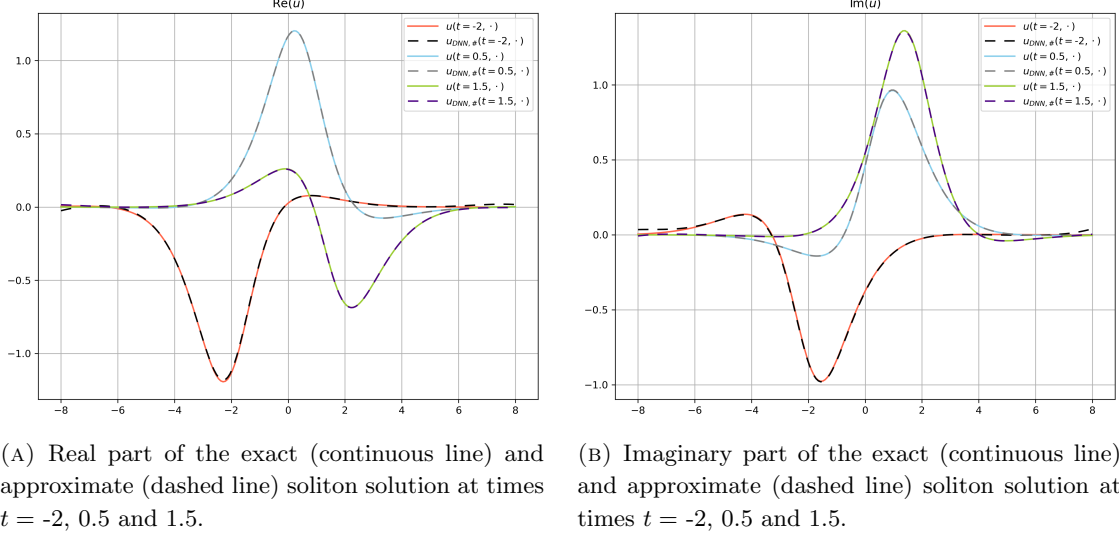


FIGURE 1. Approximation of the soliton solution in the case $c = \nu = 1$.

In Fig. 2, the evolution of the computed constants \tilde{A} , A , B , and the error of the approximation is presented in terms of the number of iterations of the numerical algorithm for the soliton solution with values $\alpha = \beta = 1$. It is noticed in Fig. 2a that the constant \tilde{A} , measuring the H^1 difference between the approximate solution at time zero and the initial data decreases in time, revealing that to get a better approximation for all posterior times, it is necessary to get very small errors at the initial time. Concerning the evolution of the computed values for the constants A and B , graphed in Figs. 2b and 2c, despite certain “explosions” produced during the evolution of the algorithm, they stabilize at some $O(1)$ value during a big part of the numerical procedure. The error function (6.1), graphed in Fig. 2d, naturally decreases through computations to achieve an $O(10^{-3})$ value.

Table 1 summarizes the elapsed time and the evolution through the iterations of the associated norms of the difference between the exact and the approximate solutions in the case of the soliton with values $c = \nu = 1$. The time interval in these cases is $[-2, 2]$, and the space interval is $[-8, 8]$. These norms are

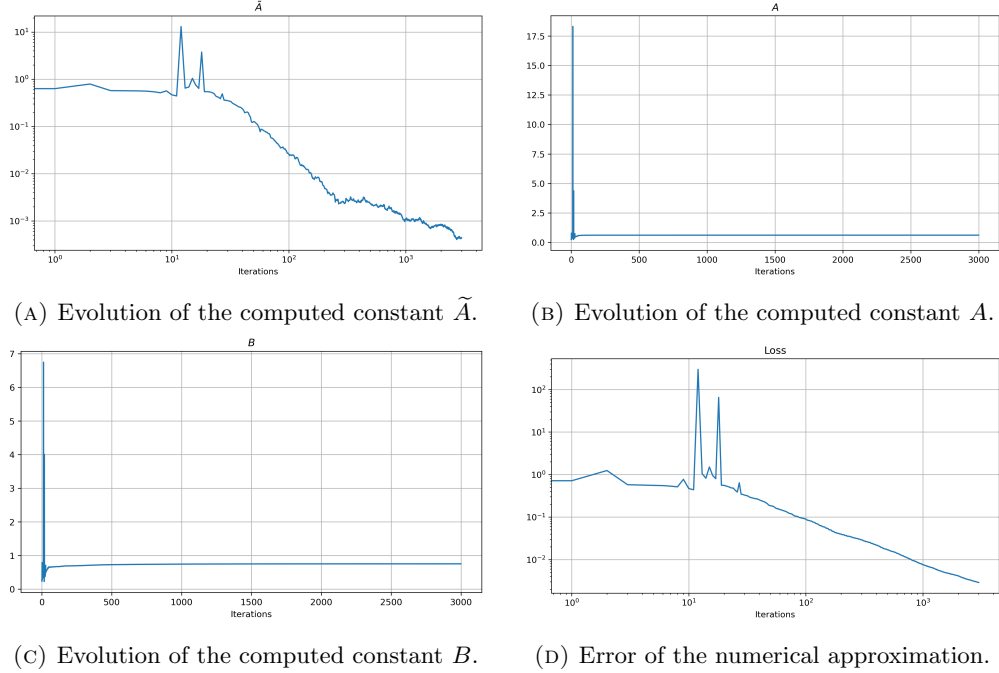


FIGURE 2. Evolution of the constants \tilde{A} , A and B and the error (6.1) during the optimization algorithm.

computed using (6.2), (6.3) and (6.4) with uniform weights equal 1, and uniform N_{test} and M_{test} given by 100. As a conclusion, from Table 1 we deduce that, during the numerical computations all the norms involved in Theorem 1.1 decreased to a value of order 10^{-2} and it takes less than one minute.

Iterations	Elapsed time [s]	error $L_t^p W_x^{1,q}$	error $L_t^\infty H^1$	error S'
100	1.846	0.434	0.515	0.668
500	9.436	0.128	0.162	0.186
1000	18.654	6.268×10^{-2}	8.161×10^{-2}	8.691×10^{-2}
3000	57.791	1.308×10^{-2}	2.051×10^{-2}	2.051×10^{-2}

TABLE 1. Computed values of the elapsed time and norms involved in Theorem 1.1, for five different number of iterations in the solitonic case.

Fig. 3 computes the $L_t^p W_x^{1,q}$ error (6.3) of the trained DNN $u_{\text{DNN},\#}$ for different admissible pairs (p,q) . The values of q are chosen uniformly as a grid of 197 points between 2 and 100, namely, $q = \frac{k}{2}$ for $k = 4, \dots, 200$. Our numerical simulations suggest that for large values of q , $\text{error}_{L_t^p W_x^{1,q}}$ is zero, and that the worst case of $\text{error}_{S'}$ in the trained DNN was dictated by the $L_t^\infty H^1$ norm or values close to it.

6.5. Kuznetsov-Ma. Even if this breather solution is not in Sobolev spaces, one can perform a similar analysis since Theorem 1.1 only consider the difference of solutions. In the case of the KM breather B_{KM} described in (6.7), we have chosen the parameter $a = \frac{3}{4}$. Notice that the larger is a , the more complicated are numerical simulations. In this case, the space region is $[-5, 5]$, and the time region $[-1, 1]$. Our results are summarized in Fig. 4, where the continuous line represents the exact solution and the dashed line is the solution computed using the proposed PINNs minimization procedure. In particular, Fig. 4a and 4b present respectively the real and imaginary parts of the computed brather solution for three different times.

In Fig. 5, the evolution of the computed constants \tilde{A} , A , B , and the error of the approximation is presented in terms of the number of iterations of the numerical algorithm for the KM solution. In this case Figs. 5a-5b-5c and 5d are in agreement with the description already found in the soliton case, with the difference that in the KM breather case there are not “explosions” in the evolution of the algorithm for \tilde{A} , A , B and the optimization loss.

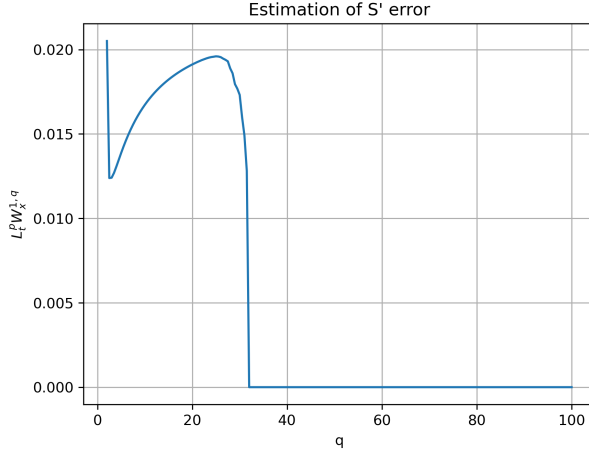
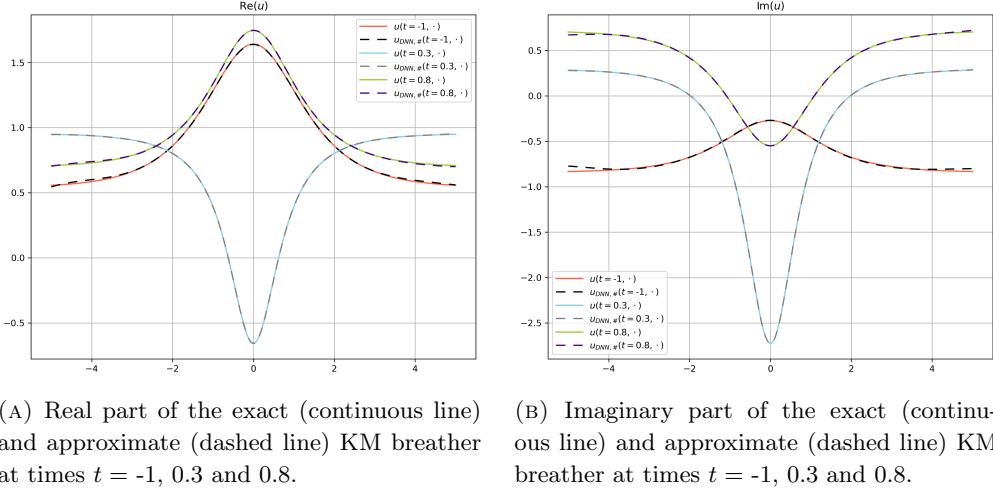


FIGURE 3. $L_t^p W_x^{1,q}$ error for different admissible pairs (p, q) in the solitonic case. The x-axis represents 100 points of q uniformly chosen between 2 and 50, and the y-axis represents the $L_t^p W_x^{1,q}$ error, where $p = \frac{4q}{q-2}$. The \mathcal{S}' error will be computed as the maximum of the $L_t^p W_x^{1,q}$ error in the grid of q .



(a) Real part of the exact (continuous line) and approximate (dashed line) KM breather at times $t = -1, 0.3$ and 0.8 .

(b) Imaginary part of the exact (continuous line) and approximate (dashed line) KM breather at times $t = -1, 0.3$ and 0.8 .

FIGURE 4. Exact (continuous line) and approximate (dashed line) KM breather at times $t = -1, 0.3$ and 0.8 .

Table 2 summarizes the elapsed time and the evolution through the iterations of the associated norms of the difference between the exact and the approximate solutions in the case of the KM breather with $a = \frac{3}{4}$. The time interval in these cases is $[-1, 1]$, and the space interval is $[-5, 5]$. These norms are computed using (6.2), (6.3) and (6.4) with uniform weights equal 1, and uniform N_{test} and M_{test} given by 100. As a conclusion, from Table 2 we deduce that, during the numerical computations all the norms involved in Theorem 1.1 decreased to a value of order 10^{-2} and it takes less than one minute.

Iterations	Elapsed time [s]	error $L_t^p W_x^{1,q}$	error $L_t^\infty H^1$	error \mathcal{S}'
100	1.823	1.649	1.669	2.560
500	9.487	0.226	0.307	0.323
1000	18.840	3.832×10^{-2}	7.079×10^{-2}	9.946×10^{-2}
3000	59.416	1.726×10^{-2}	2.922×10^{-2}	2.922×10^{-2}

TABLE 2. Computed values of the elapsed time and norms involved in Theorem 1.1, for five different number of iterations in the KM breather case.

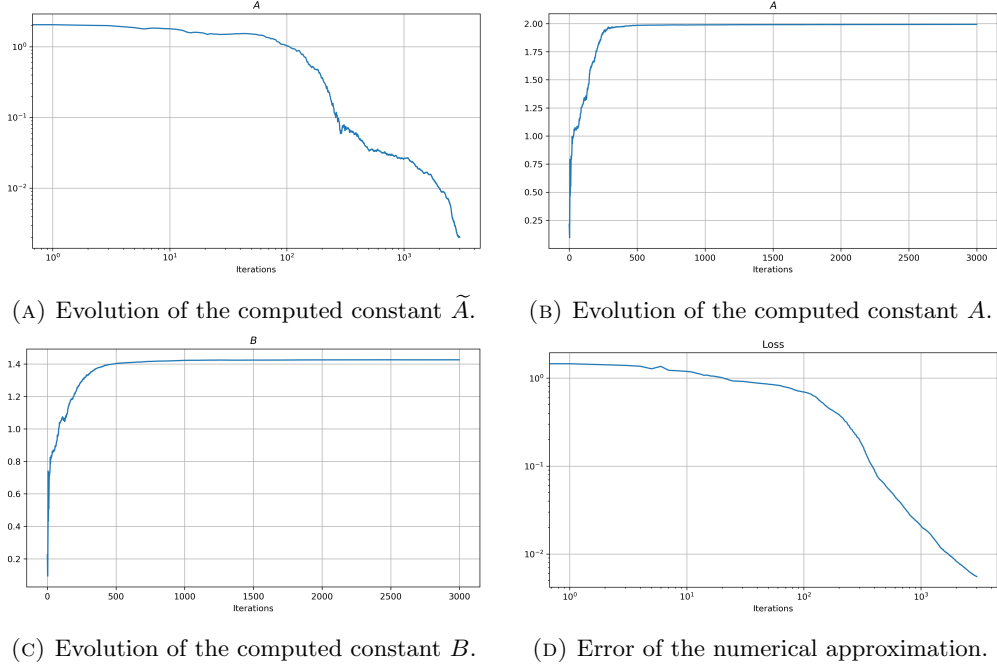


FIGURE 5. Computed evolution of the error and constants \tilde{A} , A and B in the case of the KM breather.

Later, in Table 3, we present the values of computation time, loss function (6.1), computed approximate values for \tilde{A} , A , B , and the approximate norms $L_t^p W_x^{1,q}$, $L_t^\infty H_x^1$ and \mathcal{S}' for the whole space-time computation. This is done for four different values of a . For this we fix $[-4, 4]$ the space region, $[-0.5, 0.5]$ the time region and 40 neurons per hidden layer. It is noticed that errors are usually of the order 10^{-2} . Then, the constant \tilde{A} is usually found small of the order 10^{-3} , as one might expect when approximating the solution for all times. but the norms A and B are reasonably bounded below 4. Finally, the three computed norms involved in Theorem 1.1 are suitably small, but two order higher than the value of \tilde{A} , and the \mathcal{S}' norm is dictated by the $L_t^\infty H^1$ norm.

	$a = 3/4$	$a = 1$	$a = 3/2$	$a = 2$
Elapsed Time [s]	92.791	87.610	102.096	100.890
Loss	3.605×10^{-3}	4.358×10^{-3}	6.588×10^{-3}	1.184×10^{-2}
\tilde{A}	3.466×10^{-3}	6.158×10^{-3}	2.024×10^{-3}	4.184×10^{-3}
A	2.175	2.459	2.955	3.403
B	1.589	1.690	1.851	1.987
$L_t^p W_x^{1,q}$	8.691×10^{-3}	1.055×10^{-2}	9.202×10^{-3}	2.012×10^{-2}
$L_t^\infty H_x^1$	1.848×10^{-2}	2.366×10^{-2}	2.112×10^{-2}	4.736×10^{-2}
\mathcal{S}'	1.848×10^{-2}	2.366×10^{-2}	2.112×10^{-2}	4.736×10^{-2}

TABLE 3. Computed values of the elapsed time, errors, constants and norms involved in Theorem 1.1, for four different values of a , in the KM breather case.

6.6. Peregrine breather. This is also another example of a solution with nonzero background at infinity for which the numerical approach works in a satisfactory fashion. We consider the case of the Peregrine breather B_P described in (6.6). Note that in this case there is no extra parameter that builds a family of solutions of the form of (6.6). As before, the space region is $[-10, 10]$ and the time region $[-2, 2]$. However, in this case we choose $N_4 = M_4 = 64$ and $N_5 = M_5 = 32$. Our results are summarized in Fig. 6, where the continuous line represents the exact solution and the dashed line is the solution computed using the proposed PINNs minimization procedure. In particular, Fig. 6a and 6b present respectively the real and imaginary parts of the computed breather solution for three different times.

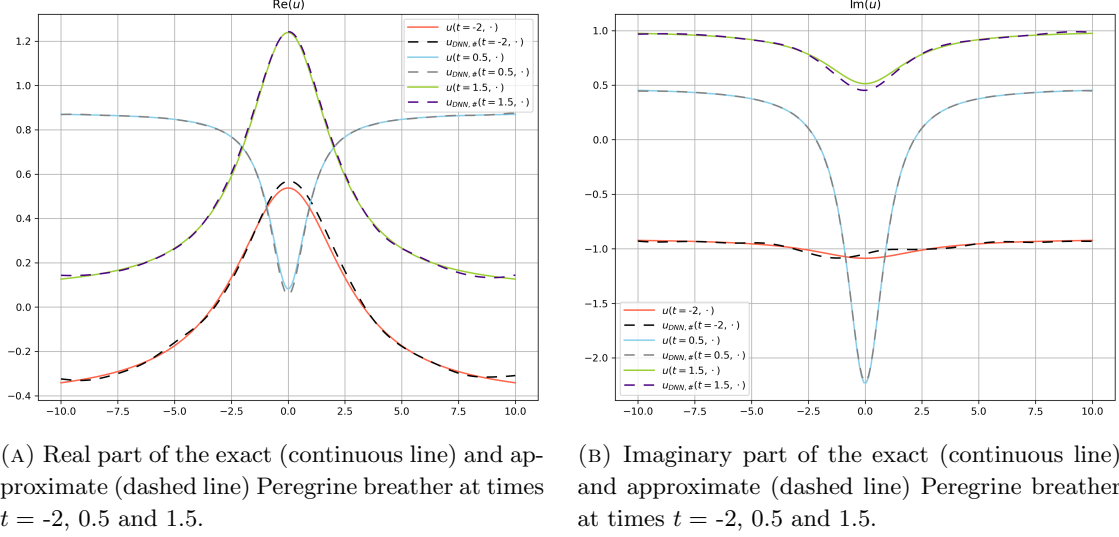


FIGURE 6. Exact (continuous line) and approximate (dashed line) Peregrine breather at times $t = -2, 0.5$ and 1.5 .

In Fig. 7, the evolution of the computed constants \tilde{A} , A , B , and the error of the approximation is presented in terms of the number of iterations of the numerical algorithm for the Peregrine solution. Figs. 7a-7b-7c and 7d are in agreement with the description already found in the previous cases.

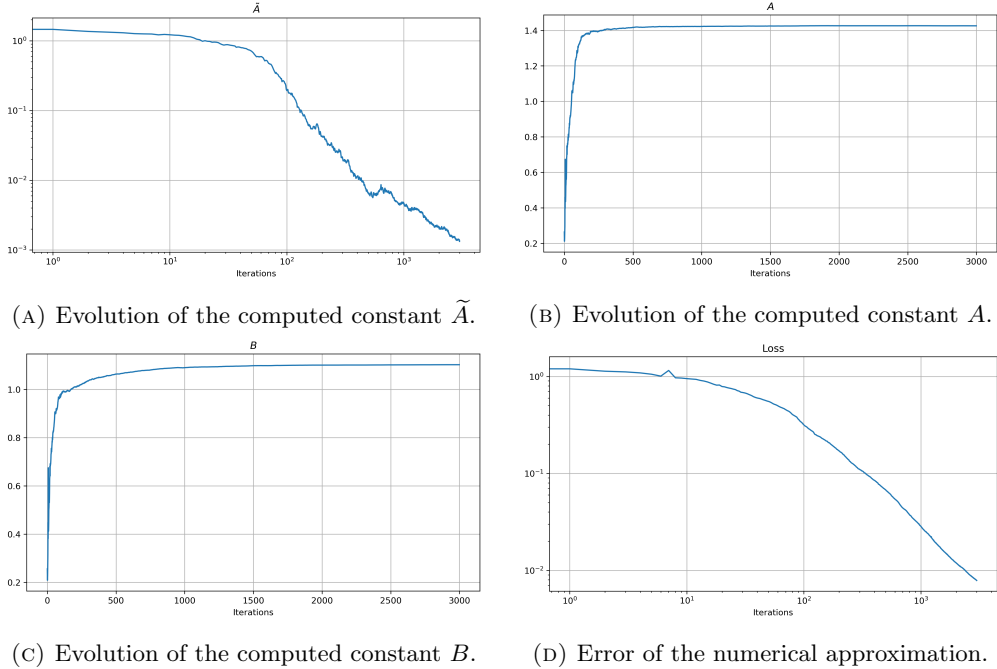


FIGURE 7. Computed evolution of the error and constants \tilde{A} , A and B in the case of the Peregrine breather.

Table 4 summarizes the elapsed time and the evolution through the iterations of the associated norms of the difference between the exact and the approximate solutions in the case of the Peregrine breather. The time interval in these cases is $[-2, 2]$, and the space interval is $[-10, 10]$. These norms are computed using (6.2), (6.3) and (6.4) with uniform weights equal 1, and uniform N_{test} and M_{test} given by 100. As a conclusion, from Table 4 we deduce that, during the numerical computations all the norms involved in Theorem 1.1 decreased to a value of order 10^{-2} and it takes around 1 minute 20 seconds. Note in this case the convergence is slower than in the previous solitonic and KM breather cases.

Iterations	Elapsed time [s]	error _{$L_t^p W_x^{1,q}$}	error _{$L_t^\infty H^1$}	error _{S'}
100	3.987	1.128	1.140	1.761
500	21.083	0.601	0.618	0.896
1000	42.992	0.222	0.242	0.330
3000	140.311	3.257×10^{-2}	4.154×10^{-2}	4.753×10^{-2}

TABLE 4. Computed values of the elapsed time and norms involved in Theorem 1.1, for five different number of iterations in the Peregrine breather case.

ν	1	3	5
Elapsed Time [s]	60.066	59.385	58.422
Loss	2.261×10^{-3}	1.756×10^{-3}	4.127×10^{-3}
\tilde{A}	3.753×10^{-4}	5.918×10^{-4}	8.153×10^{-4}
A	0.619	0.932	1.356
B	0.753	0.754	0.754
error _{$L_t^p W_x^{1,q}$}	3.959×10^{-3}	5.308×10^{-3}	7.199×10^{-3}
error _{$L_t^\infty H^1$}	5.752×10^{-3}	7.775×10^{-3}	1.632×10^{-2}
error' _{S'}	6.717×10^{-3}	8.937×10^{-3}	1.632×10^{-2}

TABLE 5. Computed values of the elapsed time, errors, constants and norms involved in Theorem 1.1, for $c = 1$ and three different values of ν , in the solitonic case.

ν	1	3	5
Elapsed Time [s]	60.066	57.748	60.053
Loss	4.388×10^{-3}	6.329×10^{-3}	5.289×10^{-3}
\tilde{A}	7.035×10^{-4}	9.144×10^{-4}	8.482×10^{-4}
A	0.975	1.337	1.861
B	1.136	1.136	1.138
error _{$L_t^p W_x^{1,q}$}	1.887×10^{-2}	1.774×10^{-2}	1.918×10^{-3}
error _{$L_t^\infty H^1$}	2.661×10^{-2}	2.823×10^{-2}	4.649×10^{-3}
error' _{S'}	2.838×10^{-2}	2.823×10^{-2}	4.649×10^{-3}

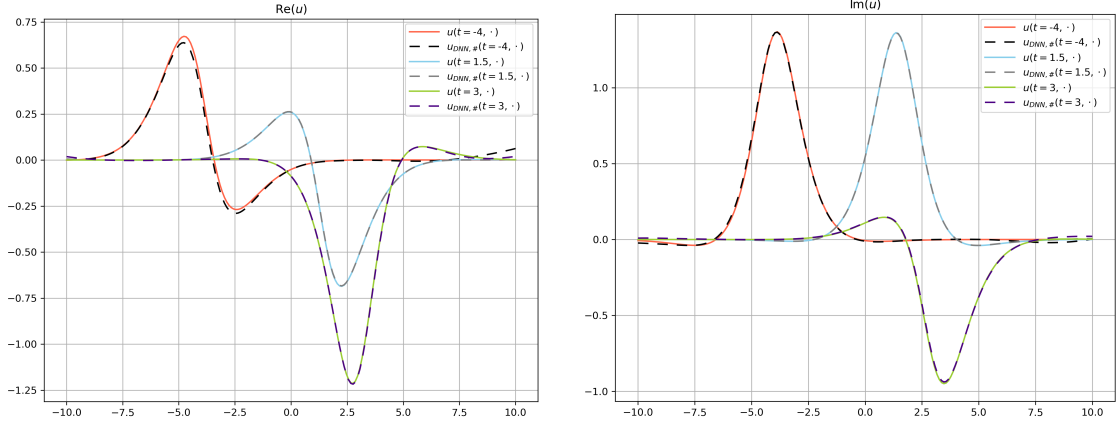
TABLE 6. Computed values of the elapsed time, errors, constants and norms involved in Theorem 1.1, for $c = 3$ and three different values of ν , in the solitonic case.

6.7. Sensitivity analysis. We will now focus in the solitonic case and by previous experiment we are hoping that these results are similar to the breather cases.

First of all we study the variation on the hyperparameters of the solution. In particular, Tables 5 and 6 present the values of computation time, loss function (6.1), computed approximate values for \tilde{A} , A , B , and the approximate norms $L_t^p W_x^{1,q}$ and $L_t^\infty H^1$ for the whole space-time computation. This is done for two and three different values of c and ν , respectively. For this we fix $[-8, 8]$ the space region and $[-1, 1]$ the time region. It is noticed that errors are usually of the order 10^{-2} . Then, the constant \tilde{A} is usually found small, as one might expect when approximating the solution for all times. but the norms A and B are reasonably bounded below 2, A increases when ν increases and B almost does not change for fixed c and variable ν . Finally, the three computed norms involved in Theorem 1.1 are suitably small, but one or two orders higher than the value of \tilde{A} .

Effect of time: In order to study the performance of the algorithm, we will change the size of the time interval. For this aim, we consider 5000 iterations, 40 neurons per hidden layer $N_4 = 128$ and $N_5 = M_4 = M_5 = 32$. Fig. 8 summarizes the performance of the solitonic case with $c = \nu = 1$ in the space region $[-10, 10]$ and the time region $[-4, 4]$, where the continuous line represents the exact solution and the dashed line is the solution computed using the proposed PINNs minimization procedure. In particular, Fig. 8a and 8b present respectively the real and imaginary parts of the computed soliton

solution for three different times. Our simulations suggest that for greater values of the time interval, the train grid needs to be fine-tuned.



(A) Real part of the exact (continuous line) and approximate (dashed line) soliton solution at times $t = -4, 1.5$ and 3 .

(B) Imaginary part of the exact (continuous line) and approximate (dashed line) soliton solution at times $t = -4, 1.5$ and 3 .

FIGURE 8. Approximation of the soliton solution in the case $c = \nu = 1$.

In this case the algorithm takes 227.659 seconds, and obtaining errors $\text{error}_{L_t^p W_x^{1,q}} = 2.081 \times 10^{-2}$, $\text{error}_{L_t^\infty H^1} = 2.739 \times 10^{-2}$, $\text{error}_{S'} = 3.051 \times 10^{-2}$, $\text{loss} = 1.453 \times 10^{-3}$ with constants $\tilde{A} = 1.654 \times 10^{-4}$, $A = 0.561$ and $B = 0.715$.

6.8. Comparison with other approximation scheme. In this section we will compare the PINN algorithm with the finite differences (FD) method implemented in [ABB13] for the Schrödinger equation (1.1). In the following comparison we will treat only with the solitonic case. As similar as in the sensitivity analysis section we will use $c \in \{1, 3\}$ and $\nu \in \{1, 3, 5\}$ and the space-time region will be $[-8, 8] \times [-1, 1]$ as before. Notice that the breather cases cannot be compared using the FD method. For these cases the time-splitting sine pseudospectral (TSSP) method, also described in [ABB13] but which will not be discussed in this paper, can be used.

Table 7 summarizes the elapsed time and the $L_t^p W_x^{1,q}$ and $L_t^\infty H_x^1$ errors in the six different pairs (c, ν) . The FD method is performed with 200 points in the space grid and 10^5 points in the time grid.

c	ν	Elapsed time [s]	$\text{error}_{L_t^p W_x^{1,q}}$	$\text{error}_{L_t^\infty H^1}$
1	1	28.477	1.265×10^{-3}	4.579×10^{-3}
1	3	28.364	6.707×10^{-3}	9.682×10^{-3}
1	5	28.041	3.521×10^{-2}	5.371×10^{-2}
3	1	28.582	1.341×10^{-2}	1.443×10^{-2}
3	3	27.960	3.523×10^{-2}	3.754×10^{-2}
3	5	27.894	9.278×10^{-2}	9.916×10^{-2}

TABLE 7. Computed values of the elapsed time and norms involved in Theorem 1.1 using the FD method, for two and three different values of c and ν , respectively, in the solitonic case.

By comparing the Tables 5 and 6 with the Table 7, the following conclusions can be made. First, although the FD method takes the half of time than our PINNs algorithm, they have the same order in the computation times. Additionally, only in the settings with $\nu = 1$ the FD method performs quite better than our algorithm. In the other settings of ν , the PINNs algorithm outperforms the FD method.

Finally, the worst case of the FD method is $c = 3, \nu = 5$: both errors have order near 10^{-1} . Even if the space-time points are increased to 300 and 1.8×10^5 , the errors decrease less than one order, namely

error $L_t^p W_x^{1,q} = 4.081 \times 10^{-2}$, error $L_t^\infty H^1 = 5.135 \times 10^{-2}$ and the elapsed time is 77.288 seconds. On the other hand, in the PINNs simulation both errors have order 10^{-3} for the setting of $(c, \nu) = (3, 5)$.

7. DISCUSSIONS AND CONCLUSIONS

7.1. Discussion. The Physics-Informed Neural Networks (PINN) methodology has recently been applied successfully to solve various nonlinear Schrödinger (NLS) equations, both analytically and numerically, in bounded domains. By integrating physical laws with neural networks, PINNs have achieved accurate solutions with minimal data requirements [SSHC22, BKM22, HaDe23, PLC21, WaYa21, ZhBa22, BMAR23, RPP19, Rai18, TSVS24]. However, these studies are limited to spatially bounded domains and do not adequately address real-world physical phenomena, which often involve slow-decaying solutions or long-range potentials in unbounded domains.

For unbounded domains, recent advancements have emerged. In [XCL21], a deep neural network (DNN) was developed to implement an absorbing boundary condition (ABC), which confines computations to a finite domain. The ABC minimizes unwanted reflections at the boundaries, effectively replicating the influence of the surrounding environment without fully discarding the unbounded regions. This method has been applied to wave and Schrödinger equations in unbounded domains. Despite their success, PINNs can be challenging to train and prone to practical issues, as demonstrated in [FWP23], particularly for wave scattering problems in unbounded domains [Colt98]. Such problems typically require sampling collocation points across an infinite domain, rendering many traditional PINN approaches unsuitable. In response, [FWP23] employed boundary integral equations (BIEs), a robust method for solving partial differential equations (PDEs) in complex or unbounded domains by representing solutions in terms of boundary values.

In [XBC23], the NLS equation on unbounded domains was addressed using a hybrid approach combining adaptive spectral and PINN methods. This approach used spectral basis functions and a priori assumptions about asymptotic spatial behavior to effectively describe the spatial dependence. Recent studies have introduced other techniques for dealing with unbounded domains: [BaEs22] introduced a similarity variable to handle infinity, while [RRCWL24] truncated the computational domain to ensure that the wave exits the domain without disturbing the upstream field.

In contrast, our approach to handling unbounded domains does not rely on external basis functions. Instead, we demonstrate how to describe the critical focusing NLS evolution on the unbounded real line by imposing a condition on the evolution of the linear part and employing appropriate approximate norms. These norms, under certain smallness assumptions, allow for an accurate approximation of NLS dynamics in this setting.

7.2. Conclusions. We have studied the subcritical nonlinear Schrödinger (NLS) equation in one dimension on the unbounded real line. The non-compact nature of this setting introduces significant challenges for approximation schemes, particularly in the context of deep neural networks (DNNs), as there is no natural restriction on the data at spatial infinity. Previous works, such as [RPP19, BKM22], have addressed NLS on bounded domains from both numerical and theoretical perspectives, advancing our understanding of dispersive solution approximations via DNN techniques.

In this paper, we propose a new approach using Physics-Informed Neural Networks (PINNs) that combines standard physical constraints with a novel component designed to handle the linear evolution of perturbed data in unbounded domains. We present what we believe are the first rigorous bounds on the associated approximation error in energy and Strichartz norms, which are fundamental in the NLS framework. Our analysis assumes the availability of suitable integration schemes capable of accurately approximating space-time norms.

Additionally, we applied this method to traveling waves, breathers, and solitons, and conducted numerical experiments that validate the effectiveness of the approximation. The results confirm that the proposed scheme performs well in capturing the dynamics of NLS solutions in unbounded domains.

REFERENCES

- [AC24] M. A. Alejo, and A. J. Corcho, *On nonexistence of NLS breathers*, arXiv:2408.09862v1 (2024).
- [AM13] M. A. Alejo, and C. Muñoz, *Nonlinear stability of mKdV breathers*. Comm.Math.Phys. 324 (1) (2013), 233–262.

[ACM24] M. A. Alejo, L. Cossetti, L. Fanelli, C. Muñoz, and N. Valenzuela, *Bounds on the approximation error for deep neural networks applied to dispersive models: Nonlinear Schrödinger*, preprint under preparation (2024).

[AFM19] M. A. Alejo, L. Fanelli, and C. Muñoz, *The Akhmediev breather is unstable*. São Paulo J. Math. Sci. 13 (2019), no. 2, 391–401.

[AFM21] M. A. Alejo, L. Fanelli, and C. Muñoz, *Stability and instability of breathers in the $U(1)$ Sasa-Satsuma and nonlinear Schrödinger models*. Nonlinearity 34 (2021), no. 5, 3429–3484.

[AFM20] M. A. Alejo, L. Fanelli, and C. Muñoz, *Review on the stability of the Peregrine and related breathers*, Frontiers in Physics, section Mathematical and Statistical Physics, Mini-Review, Front. Phys., 24 (2020).

[AMP17] M. A. Alejo, C. Muñoz and J.M. Palacios, *On the variational structure of breather solutions I: sine-Gordon equation*. Journal of Mathematical Analysis and Applications Vol.453/2 (2017).

[ABB13] X. Antoine, W. Bao, and C. Besse, *Computational Methods for the Dynamics of the Nonlinear Schrödinger/Gross-Pitaevskii Equations*. Computer Physics Communications, vol. 184, no. 12, (2013), pp. 2621–33. <https://doi.org/10.1016/j.cpc.2013.07.012>.

[BKM22] G. Bai, U. Koley, S. Mishra, and R. Molinaro, *Physics informed Neural Networks (PINNs) for approximating nonlinear dispersive PDEs*, J. Comp. Math., 39 (2021), pp. 816–847 [10.4208/jcm.2101-m2020-0342](https://doi.org/10.4208/jcm.2101-m2020-0342).

[BMAR23] C. Bajaj, L. McLennan, T. Andeen and A. Roy, *Recipes for when physics fails: recovering robust learning of physics informed neural networks*, Mach. Learn.: Sci. Technol. 4 (2023) 015013.

[BaEs22] H. Bararnia and M. Esmaeilpour, *On the application of physics informed neural networks (PINN) to solve boundary layer thermal-fluid problems*, International Communications in Heat and Mass Transfer 132 (2022) 105890.

[BeJe19] C. Beck and A. Jentzen. *Machine learning approximation algorithms for high-dimensional fully nonlinear partial differential equations and second-order backward stochastic differential equations*. Journal of Nonlinear Science, 29(4), 1563–1619, 2019.

[BBGJJ21] C. Beck, S. Becker, P. Grohs, N. Jaafari and A. Jentzen. *Solving the Kolmogorov PDE by Means of Deep Learning*. Journal of Scientific Computing, vol. 88, no. 3, July 2021. <https://doi.org/10.1007/s10915-021-01590-0>.

[BHHJK20] C. Beck, F. Hornung, M. Hutzenthaler, A. Jentzen, and T. Kruse. *Overcoming the curse of dimensionality in the numerical approximation of Allen-Cahn partial differential equations via truncated full-history recursive multilevel Picard approximations*. Journal of Numerical Mathematics, 28(4):197–222, dec 2020.

[BHJK23] C. Beck, M. Hutzenthaler, A. Jentzen, and B. Kuckuck, *An overview on deep learning-based approximation methods for partial differential equations*. Discrete Contin. Dyn. Syst. Ser. B 28 (2023), no. 6, 3697–3746.

[BGJ20] J. Berner, P. Grohs and A. Jentzen. *Analysis of the generalization error: Empirical risk minimization over deep artificial neural networks overcomes the curse of dimensionality in the numerical approximation of Black–Scholes partial differential equations*. SIAM J. Math. Data Science, 2(3), 631–657, 2020.

[BMW94] B. Birnir, H.P. McKean, A. Weinstein, *The rigidity of sine-Gordon breathers*, Comm. Pure Appl. Math. 47, 1043–105, (1994).

[BDPS24] A. Bonito, R. DeVore, G. Petrova, and J. W. Siegel, *Convergence and error control of consistent PINNs for elliptic PDEs*, arXiv:2406.09217

[Bou99] J. Bourgain, *Global well posedness of defocusing critical nonlinear Schrödinger equation in the radial case*, Jour.AMS **12** (1999) 145–171.

[Cas22] J. Castro. *Deep Learning schemes for parabolic nonlocal integro-differential equations*. Partial Differ. Equ. Appl. 3, no. 6, 77, 2022.

[Cas23] J. Castro, *The Kolmogorov infinite dimensional equation in a Hilbert space via deep learning methods*. J. Math. Anal. Appl. 527 (2023), no. 2, Paper No. 127413, 40 pp.

[CMV24] J. Castro, C. Muñoz and N. Valenzuela. *The Calderón’s problem via DeepONets*. Vietnam J. Math. 2024 (Carlos Kenig’s 70 anniversary). <https://doi.org/10.1007/s10001-023-00674-8>

[Caz89] T. Cazenave, *An introduction to Nonlinear Schrödinger equations*. Textos de Métodos Matemáticos **22**, UFRJ (1989).

[Caz03] T. Cazenave, *Semilinear Schrödinger equations*. Courant Lecture Notes in Mathematics 10. Providence, RI: (AMS); Courant Institute of Mathematical Sciences (2003).

[ChCh95] T. Chen and H. Chen. *Universal approximation to nonlinear operators by neural networks with arbitrary activation functions and its application to dynamical systems*. IEEE Transactions on Neural Networks, 6 (4): 911–917, 1995.

[Colt98] D.L. Colton and R. Kress, *Inverse acoustic and electromagnetic scattering theory*, **93**, Springer, 1998.

[RyMi22] T. De Ryck and S. Mishra. *Error Analysis for Physics-Informed Neural Networks (PINNs) Approximating Kolmogorov PDEs*. Advances in Computational Mathematics, vol. 48, no. 6, Nov. 2022. <https://doi.org/10.1007/s10444-022-09985-9>.

[RJM22] T. De Ryck, A. D. Jagtap and S. Mishra. *Error estimates for physics informed neural networks approximating the Navier-Stokes equations*. arXiv preprint arXiv:2203.09346, 2022.

[RMM24] T. De Ryck, S. Mishra, and R. Molinaro, *wPINNs: Weak Physics Informed Neural Networks for Approximating Entropy Solutions of Hyperbolic Conservation Laws*, SIAM Journal on Numerical Analysis Vol. 62, Iss. 2 (2024).

[FWP23] Z. Fang, S. Wang, P. Perdikaris, *Learning Only On Boundaries: a Physics-Informed Neural operator for Solving Parametric Partial Differential Equations in Complex Geometries*, arXiv:2308.12939

[FMR23] A. Ferrer-Sánchez, J.D. Martín-Guerrero, R. Ruiz de Austria, A. Torres-Forné and J.A. Font, *Gradient-Annihilated PINNs for Solving Riemann Problems: Application to Relativistic Hydrodynamics* arXiv:2305.08448.

[Fle13] R. Fletcher. *Practical methods of optimization*. John Wiley & Sons, (2013).

[GiVe79] J. Ginibre and G. Velo. *On the class of nonlinear Schrödinger equations I. The Cauchy problem, general case*, J. Funct. Anal. 32(1), 33-72 (1979).

[GiVe85] J. Ginibre and G. Velo. *Scattering theory in the energy space for the class of nonlinear nonlinear Schrödinger equations*, J. Math. Pures Appl. 64, 363-401 (1985).

[GoSc21] L. Gonon and C. Schwab. *Deep ReLU neural networks overcome the curse of dimensionality for partial integro-differential equations*. arXiv preprint arXiv:2102.11707, 2021.

[GrHe21] P. Grohs and L. Herrmann. *Deep neural network approximation for high-dimensional elliptic PDEs with boundary conditions*. IMA Journal of Numerical Analysis, 2021. <https://doi.org/10.1093/imanum/drab031>.

[GHJW18] P. Grohs, F. Hornung, A. Jentzen, and P. Von Wurstemberger. *A proof that artificial neural networks overcome the curse of dimensionality in the numerical approximation of Black-Scholes partial differential equations*. arXiv preprint arXiv:1809.02362, 2018.

[GRPK19] M. Julian, M. Raissi, P. Perdikaris and G. Karniadakis. *Machine Learning of Space-Fractional Differential Equations*. SIAM Journal on Scientific Computing, vol. 41, no. 4, Jan. 2019, pp. A2485-2509. <https://doi.org/10.1137/18m1204991>.

[Had23] M.A. Haddou, *Quasi-normal modes of near-extremal black holes in dRGT massive gravity using Physics-Informed Neural Networks (PINNs)*, arXiv:2303.02395 (2023).

[HJE18] W. E. J. Han, A. Jentzen and W. E. *Solving High-Dimensional Partial Differential Equations Using Deep Learning*. Proceedings of the National Academy of Sciences, vol. 115, no. 34, Aug. 2018. <https://doi.org/10.1073/pnas.1718942115>.

[HaJe17] W. E., J. Han and A. Jentzen. *Deep learning-based numerical methods for high-dimensional parabolic partial differential equations and backward stochastic differential equations*. Commun. Math. Stat. 5(4), 349-380, 2017.

[HaDe23] L. Harcombe, Q. Den *Physics-informed neural networks for discovering localised eigenstates in disordered media*, Jour. Comp. Sci. 73 (2023) 102136.

[Hor91] K. Hornik. *Approximation Capabilities of Multilayer Feedforward Networks*, Neural Networks, Vol. 4, pp. 251-257. 1991.

[HPW20] C. Huré, H. Pham, and X. Warin. *Deep backward schemes for high-dimensional nonlinear PDEs*, Math. Comp. 89, no. 324, 1547-1579, 2020.

[HJKW20b] M Hutzenthaler, A. Jentzen, T. Kruse, T. A. Nguyen, and P. Von Wurstemberger. *Overcoming the curse of dimensionality in the numerical approximation of semilinear parabolic partial differential equations*. Proc. Royal Soc. A: Math. Phys. Eng. Sciences, 476 (2244):20190630, Dec. 2020.

[JKW23] A. Jentzen, B. Kuckuck, P. V. Wurstemberger, *Mathematical Introduction to Deep Learning: Methods, Implementations, and Theory*, preprint arXiv <https://arxiv.org/pdf/2310.20360.pdf> (2023).

[JSW21] A. Jentzen, D. Salimova, and T. Welti. *A proof that deep artificial neural networks overcome the curse of dimensionality in the numerical approximation of Kolmogorov partial differential equations with constant diffusion and nonlinear drift coefficients*. Comm. Math. Sciences, vol. 19, no. 5, 2021, pp. 1167-1205. <https://doi.org/10.4310/cms.2021.v19.n5.a1>.

[JORS24] L. Ji, A. Ostermann, F. Rousset, and K. Schratz, *Low regularity full error estimates for the cubic nonlinear Schrödinger equation*. SIAM J. Numer. Anal. 62 (2024), no. 5, 2071–2086.

[JORS24bis] L. Ji, A. Ostermann, F. Rousset, and K. Schratz, *Low regularity error estimates for the time integration of 2D NLS*. IMA Journal on Numerical Analysis 00 (2024), 1-37.

[KMPT24] D. A. Kaltsas, L. Magafas, P. Papadopoulou, and G. N. Throumoulopoulos, *Multi-soliton solutions and data-driven discovery of higher-order Burgers' hierarchy equations with physics informed neural networks*, arXiv:2408.07027 (2024).

[KKLPWY21] G. E. Karniadakis, I. G. Kevrekidis, L. Lu, P. Perdikaris, S. Wang, and L. Yang, *Physics-informed machine learning*, Nature Reviews Physics, 3(6), 422-440 (2021).

[KK24] S. Kathane and S. Karagadde, *A Physics Informed Neural Network (PINN) Methodology for Coupled Moving Boundary PDEs*, arXiv:2409.10910 (2024).

[KoWh19] M. J. Kochenderfer and T. A. Wheeler. *Algorithms for Optimization*, The MIT Press, (2019).

[Kuz77] E. Kuznetsov, *Solitons in a parametrically unstable plasma*. Sov. Phys. - Dokl. **22**, p.507-8 (1977).

[Ma79] Y-C. Ma, *The perturbed plane-wave solutions of the cubic Schrödinger equation*. Stud. Appl. Math. **60**, p.43-58 (1979).

[LLF98] I. E. Lagaris, A. Likas, and D. I. Fotiadis. *Artificial neural networks for solving ordinary and partial differential equations*. IEEE Transactions on Neural Networks, 9(5):987-1000, 1998.

[LLP00] I. E. Lagaris, A. Likas, and P. G. D. *Neural-network methods for boundary value problems with irregular boundaries*. IEEE Transactions on Neural Networks, 11:1041-1049, 2000.

[LLPS93] M. Leshno, I. V. Ya. Lin, A. Pinkus, and S. Schocken, *Multilayer Feedforward Networks With a Nonpolynomial Activation Function Can Approximate Any Function*, Neural Networks, Vol. 6, pp. 861–867 (1993).

[LiPo14] F. Linares and G. Ponce, *Introduction to nonlinear dispersive equations*. Springer. 2nd ed. (2014).

[LBH15] Y. LeCun, Y. Bengio, and G. Hinton, *Deep learning*, Nature Vol. 521 28 May 2015, doi:10.1038/nature14539.

[LNPC24] N.J. Lobos, A.M. Neube, R. C. Pantig and A.S. Cornell, *Analyzing the effect of higher dimensions on the black hole silhouette, deflection angles, and PINN approximated quasinormal modes*, arXiv:2406.08078.

[LBK24] B. Lorenz, A. Bacho and G. Kutyniok. *Error Estimation for Physics-informed Neural Networks Approximating Semilinear Wave Equations*. Preprint arXiv:2402.07153 <https://arxiv.org/abs/2402.07153> (2024).

[LJK21] L. Lu, P. Jin and G. Em Karniadakis. *Learning Nonlinear Operators via DeepONet Based on the Universal Approximation Theorem of Operators*. Nature Machine Intelligence, vol. 3, no. 3, Mar. 2021. <https://doi.org/10.1038/s42256-021-00302-5>.

[LMR20] K. O. Lye, S. Mishra, and D. Ray. *Deep learning observables in computational fluid dynamics*. Journal of Computational Physics, page 109339, 2020.

[MJK20] Z. Mao, A. D. Jagtap, and G. E. Karniadakis. *Physics-informed neural networks for high-speed flows*. Computer Methods in Applied Mechanics and Engineering, 360:112789, 2020.

[MiMo20] S. Mishra, and R. Molinaro, *Estimates on the generalization error of Physics Informed Neural Networks (PINNs) for approximating a class of inverse problems for PDEs*, arXiv:2007.01138 (2020).

[MiMo22] S. Mishra, and R. Molinaro, *Estimates on the generalization error of physics-informed neural networks for approximating PDEs*, IMA Journal of Numerical Analysis (2023) Vol. 43, 1–43.

[Wad73] M. Wadati, *The Modified Korteweg-de Vries Equation*, Jour. Phys. Soc. Japan, 34, 1289-1296 (1973).

[MMN20] B. Moseley, A. Markham, and T. Nissen-Meyer. *Solving the wave equation with physics-informed deep learning*. Preprint arXiv arXiv:2006.11894, <https://arxiv.org/abs/2006.11894> (2020).

[Mu17] C. Muñoz, *Instability in nonlinear Schrödinger breathers*. Proyecciones 36 (2017), no. 4, 653–683.

[MuVa24] C. Muñoz, and N. Valenzuela, *Bounds on the approximation error for deep neural networks applied to dispersive models: Nonlinear waves*, Preprint arXiv 2024 <https://arxiv.org/abs/2405.13566>.

[PLK19] G. Pang, L. Lu, and G. E. Karniadakis. *Fpinns: Fractional physics-informed neural networks*. SIAM Journal of Scientific Computing, 41:A2603-A2626, 2019.

[PeCh24] Wei-Qi Peng, Yong Chen, *Symmetric PINN for integrable nonlocal equations: Forward and inverse problems*, Chaos 34, 043124 (2024)

[Per83] D.H. Peregrine, *Water waves, nonlinear Schrödinger equations and their solutions*. J. Aust. Math. Soc. B 25 p.16-43, (1983).

[PLC21] J. Pu, J. Li and Y. Chen, *Solving localized wave solutions of the derivative nonlinear Schrodinger equation using an improved PINN method*, Nonlinear Dyn 105, 1723-1739 (2021).

[Rai18] M. Raissi, *Deep hidden physics models: Deep learning of nonlinear partial differential equations*. Journal of Machine Learning Research, 19(1), 932-955 (2018).

[RaKa18] M. Raissi and G. E. Karniadakis. *Hidden physics models: Machine learning of nonlinear partial differential equations*. Journal of Computational Physics, 357:125-141, 2018.

[RPK17] M. Raissi, P. Perdikaris, and G. E. Karniadakis, *Machine learning of linear differential equations using Gaussian processes*, J. Comp. Phys., 348 (2017), pp. 683-693, <https://doi.org/10.1016/j.jcp.2017.07.050>.

[RPP19] M. Raissi, P. Perdikaris, and G. E. Karniadakis. *Physics-informed neural networks: A deep learning framework for solving forward and inverse problems involving nonlinear partial differential equations*. Journal of Computational Physics, 378:686-707, 2019.

[RHS22] M. Rasht-Behesht, C. Huber, K. Shukla, G. E. Karniadakis, *Physics-informed Neural Networks (PINNs) for Wave Propagation and Full Waveform Inversions*, Jour. Geophysical Research: Solid Earth, 127, e2021JB023120. (2022).

[RRSL23] P. Ren, C. Rao, H. Sun, and Y. Liu, *Physics-informed neural network for seismic wave inversion in layered semi-infinite domain*. In arXiv:2305.05150.

[RRCWL24] P. Ren, C. Rao, S. Chen, J. X. Wang, H. Sun, Y. Liu, *SeismicNet: Physics-informed neural networks for seismic wave modeling in semi-infinite domain*, Computer Physics Communications 295 (2024) 109010.

[Szc23] S. Saqlain, W. Zhu, E. G. Charalampidis, P. G. Kevrekidis, *Discovering Governing Equations in Discrete Systems Using PINNs* Comm. Nonlin. Science and Num. Sim.126, 107498 (2023).

[SY74] J. Satsuma, and N. Yajima, *Initial Value Problems of One-Dimensional Self-Modulation of Nonlinear Waves in Dispersive Media*, Supplement of the Progress of Theoretical Physics, No. 55, 284-306, (1974).

[SSHc22] K. Shah, P. Stiller, N. Hoffmann and A. Cangi *Physics-Informed Neural Networks as Solvers for the Time-Dependent Schrödinger Equation* arXiv:2210.12522.

[TaVi05] T. Tao and M. Visan, *Stability of Energy-Critical Nonlinear Schrodinger Equations in High Dimensions*, Electronic Journal of Differential Equations **2005** (2005), no. 118, 1-28.

[TSVS24] K. Thulasidharan,1 N. Sinthuja,2 N. Vishnu Priya,3 and M. Senthilvelan, *On examining the predictive capabilities of two variants of PINN in validating localised wave solutions in the generalized nonlinear Schrödinger equation*, arxiv 2407.07415v1

[Tsu87] Y. Tsutsumi, *L^2 -solutions for nonlinear Schrödinger equations and nonlinear groups*. Funkcial Ekvac. 30: 115-25. 17, (1987).

[Val22] N. Valenzuela. *A new approach for the fractional Laplacian via deep neural networks*. Preprint arXiv:2205.05229 <https://arxiv.org/abs/2205.05229> (2022).

[Val23] N. Valenzuela, *A numerical approach for the fractional Laplacian via deep neural networks*, preprint arXiv:2308.16272 <https://arxiv.org/abs/2308.16272>, to appear in the 12th Computing Conference 2024 (London).

[WaYa21] L. Wang, Z. Yan, *Data-driven rogue waves and parameter discovery in the defocusing NLS equation with a potential using the PINN deep learning*, Phys. Lett. A 404, 127408 (2021).

[WWLL23] J. Wang, X. Wang, J. Li and B. Liu, *Data Generation-based Operator Learning for Solving Partial Differential Equations on Unbounded Domains*, arXiv:2309.02446

[XBC23] M. Xia 1, L. Böttcher, and T. Chou, *Spectrally adapted physics-informed neural networks for solving unbounded domain problems*, Mach. Learn.: Sci. Technol. 4 (2023) 025024.

[XCL21] C. Xie, J. Chen, and X. Li. *A machine-learning method for time-dependent wave equations over unbounded domains*. arXiv:2101.05807.

[Yar17] D. Yarotsky, *Error bounds for approximations with deep ReLU networks*, Neural Networks Volume 94, (2017), 103–114.

[ZYX22] Y. Zang, Z. Yu, K Xu, X Lan, M Chen, S Yang and H Chen, *Principle-driven Fiber Transmission Model based on PINN Neural Network*, Jour. Lightwave Technology Vol. 40(2), 404-414 (2022).

[ZhBa22] C.J. Zhang and Y.X. Bai, *A Novel Method for Solving Nonlinear Schrödinger Equation with a Potential by Deep Learning*. Jour.Appl. Math. Phys, 10, (2022) 3175-3190.

[Zer22] U. Zerbinati, *PINNs and GALS: A Priori Error Estimates for Shallow Physics Informed Neural Networks Applied to Elliptic Problems*, IFAC-PapersOnLine Volume 55 (20), 61-66 (2022).

[ZFWCQ21] G-Zhou Wu, Y Fang, Y-Y Wang, G-Cheng Wu, C-Qing Dai, *Predicting the dynamic process and model parameters of the vector optical solitons in birefringent fibers via the modified PINN*, Chaos, Solitons & Fractals Volume 152: 111393, (2021).

[ZKCK22] W. Zhu, W. Khademi, E.G. Charalampidis, and P.G. Kevrekidis, *Neural Networks Enforcing Physical Symmetries in Nonlinear Dynamical Lattices: The Case Example of the Ablowitz-Ladik Model*. Physica D: Nonlinear Phenomena, 434:133264, (2022).

DEPARTAMENTO DE MATEMÁTICAS. UNIVERSIDAD DE CÓRDOBA, CÓRDOBA, SPAIN.

Email address: malejo@uco.es

IKERBASQUE AND UPV/EHU, APTDO. 644, 48080, BILBAO, SPAIN

Email address: lucrezia.cossetti@ehu.eus

IKERBASQUE & UNIVERSIDAD DEL PAÍS VASCO/EUSKAL HERRIKO UNIBERTSITATEA, UPV/EHU & BCAM, APTDO. 644, 48080, BILBAO, SPAIN

Email address: luca.fanelli@ehu.es

DEPARTAMENTO DE INGENIERÍA MATEMÁTICA AND CENTRO DE MODELAMIENTO MATEMÁTICO (UMI 2807 CNRS), UNIVERSIDAD DE CHILE.

Email address: cmunoz@dim.uchile.cl

DEPARTAMENTO DE INGENIERÍA MATEMÁTICA, UNIVERSIDAD DE CHILE.

Email address: nvalenzuela@dim.uchile.cl